A Comparison of Georges Bank, Gulf of Maine and New England Shelf Tidal Dynamics

WENDELL S. BROWN

Ocean Process Analysis Laboratory, Department of Earth Sciences, University of New Hampshire, Durham, NH 03824

(Manuscript received 23 March 1983, in final form 12 September 1983)

ABSTRACT

The semidiurnal tidal currents associated with the near-resonant response of the Gulf of Maine–Bay of Fundy system are amplified over the relatively shallow depths of Georges Bank, thus leading to enhanced energy dissipation, vertical mixing and secondary flows on the Bank. Within the western Gulf of Maine the tidal sea level amplitudes are larger but currents are less energetic than those observed on Georges Bank, while on the New England shelf the tidal response is the least energetic of the three regions. In this paper we explore some of the details of the tidal dynamics in these three very different tidal regimes by estimating terms in the volume-integrated momentum equations using observations of current and bottom pressure. The computations are performed for the M_2 semidiurnal tidal constituent, which is the dominant tide in all of the regions, and are presented in terms of an instantaneous "stress" balance.

Results show that in the across-isobath direction on Georges Bank the M_2 inertial term is balanced principally by the sum of the Coriolis and pressure gradient terms plus a small residual term, while in the along-isobath direction the principal balance is between the inertial and Coriolis terms. Even in this region of relatively high currents the nonlinear terms are found to be small in both directions, thus justifying the use of monochromatic input data. The instantaneous dynamic balances and the clockwise rotary elliptical currents are quantitatively consistent with the signature of an across-isobath propagating, forced gravitational-gyroscopic progressive wave which is strongly influenced by bottom slope. In the western Gulf of Maine a sum of the inertial and Coriolis terms in both the along- and across-isobath directions is balanced by the relatively large pressure gradient terms—dynamic balances that are consistent with those of a rotary standing wave. The distribution of counterclockwise rotary elliptical currents suggest the presence of a reflected Kelvin wave in the western Gulf. On the less energetic New England shelf the across-isobath inertial term is balanced by a sum of the Coriolis and pressure gradient terms as found on Georges Bank. However in the along-isobath direction, unlike Georges Bank, the same dynamical balance is found because of the importance of coastline irregularities in producing significant along-isobath tidal pressure gradients. The tidal response of the New England shelf combines the dynamical characteristics of those on Georges Bank and on the New Jersey shelf to the southwest and is less easily described in terms of the simple forced-wave models that are reasonably successful in the adjacent regions.

The Georges Bank and Gulf of Maine observed tides are compared with the Greenberg fine-grid numerical results with generally good overall result. Some small systematic differences, which are found, may be due to the way friction is specified in the numerical model. Other results concerning the vertical structure and frictional character of Georges Bank tidal flow, which are presented here, suggest that the continued study of the way tidal energy dissipation is computed is warranted.

1. Introduction

The tidal response of the Atlantic Ocean is clearly dominated by the M_2 semidiurnal constituent, which can be described in terms of a counterclockwise amphidromic system with its node in the central North Atlantic as shown in Fig. 1. An M_2 cotidal chart presented in Fig. 2 shows more clearly how the southwestward propagating deep-ocean tidal wave is distorted by the presence of the Gulf of Maine and the northeastern American continental shelf. Much of the distortion is related to the near-resonant condition of the Gulf of Maine at the semidiurnal frequency. The energy dissipation associated with the relatively large tidal currents in the Bay of Fundy and on Georges Bank make this area one of the more dissipative in the North Atlantic. Despite the large tidal amplitudes in the western Gulf of Maine the tidal currents there are smaller than Georges Bank currents with a correspondingly reduced energy dissipation. The New England shelf south of Block Island Sound is characterized by the typical shelf tidal amplitudes like those on Georges Bank and tidal currents more like those in the western Gulf of Maine. Thus the tidal characteristics of these different regions on the northeast American continental shelf suggest that the tidal dynamics found in each of these regions are likely to differ. We explore those differences in this paper.

The tidal response of the northeastern American continental shelf and the Gulf of Maine is driven principally by the deep ocean tides at the edge of the shelf with direct astronomical forcing being less important. Garrett (1972) has shown that it is the entire Gulf of Maine–Bay of Fundy basin which is in near-resonance

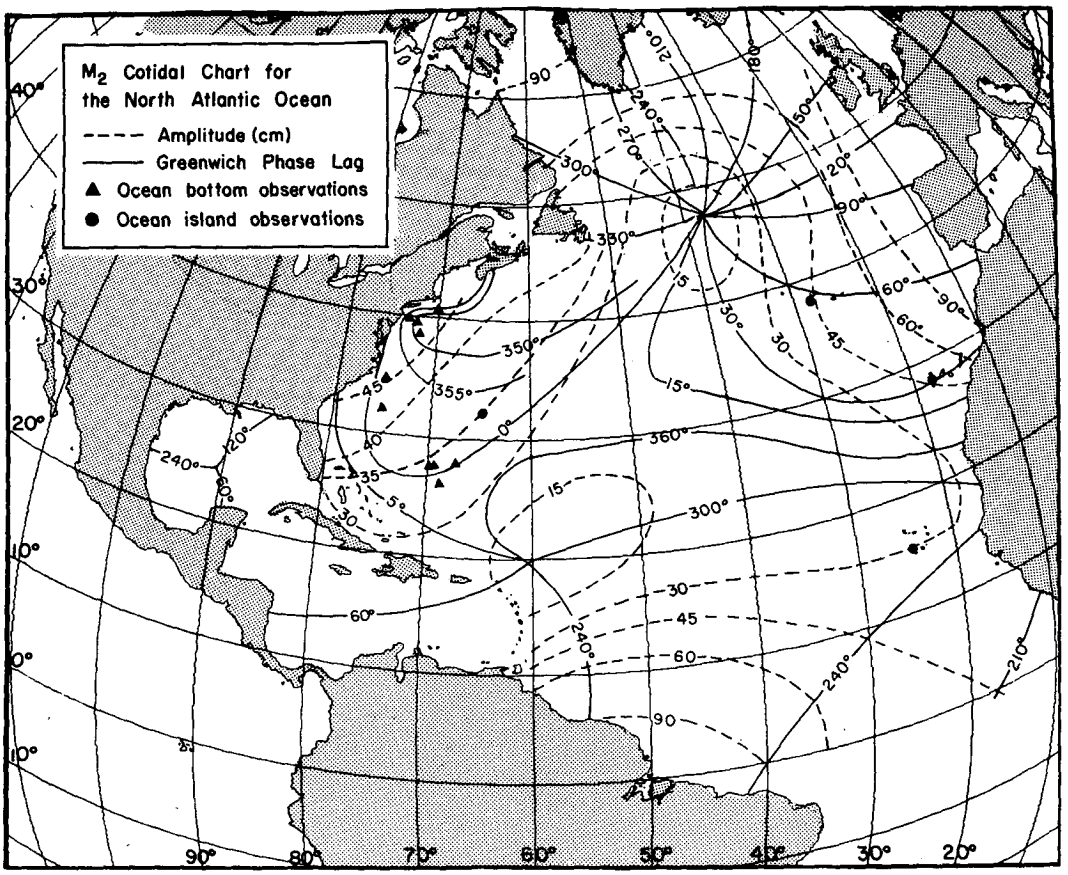

FIG. 1. An M_2 cotidal chart of the North Atlantic Ocean (after Beaumont and Boutilier, 1978).

with oceanic semidiurnal forcing. The amplified Gulf of Maine tidal amplitudes, which characterize this resonance, require the large tidal transports flowing over the relatively shallow Georges Bank. Thus it is not surprising that Greenberg (1979) finds large tidal dissipation rates on Georges Bank as well as in the Bay of Fundy where currents are also amplified. For dynamical reasons, which will be explored here, these relatively high tidal dissipation rates are not found in the western Gulf of Maine nor on the New England shelf.

In this paper the details of the tidal dynamics on the south flank of Georges Bank, in the western Gulf of Maine and on the New England shelf are explored. In Section 2 the details of how the depth-averaged equations of motion are integrated over an area are presented. In Section 3 we present the tidal characteristics of the three regions for which data sets exist and show how the terms in the "stress balance" derived in Section 2 can be estimated from the observations. In Section 4 the dynamical implications of these results are discussed.

2. Theoretical considerations

The terms in the volume-integrated momentum equations are estimated as discussed in the next section, using bottom pressure and current measurements at stations located in Fig. 3. The following summarizes the development of the relations used in estimating these momentum terms.

First we consider a coordinate system with x aligned across the isobaths onshelf, y along the isobaths alongshelf towards the west and z upwards with the corresponding velocity components u, v and w. When the continuity relation

$$\frac{\partial u}{\partial x}+\frac{\partial v}{\partial y}+\frac{\partial w}{\partial z}=0 \tag{1}$$

is vertically integrated between the bottom at $z=h(x, y)$, and the surface at $z=\eta$, it can be written

$$\frac{\partial \bar{u}}{\partial x}+\frac{\partial \bar{v}}{\partial y}+\frac{\partial(\eta+h)}{\partial t}=0, \tag{2}$$

where the notation for vertical integration, $\overline{(\ )} \equiv \int_{-h}^{\eta}(\ )dz$, is used. When (1) is multiplied first by and second by v and then added to the appropriate horizontal momentum equation, we can write

$$\frac{\partial u}{\partial t}+\frac{\partial u^2}{\partial x}+\frac{\partial uv}{\partial y}+\frac{\partial uw}{\partial z}-fv$$

$$=-\frac{1}{\rho}\frac{\partial \hat{p}}{\partial x}+\frac{1}{\rho}\left(\frac{\partial \sigma_{xx}}{\partial x}+\frac{\partial \tau_{yx}}{\partial y}+\frac{\partial \tau_{zx}}{\partial z}\right), \tag{3}$$

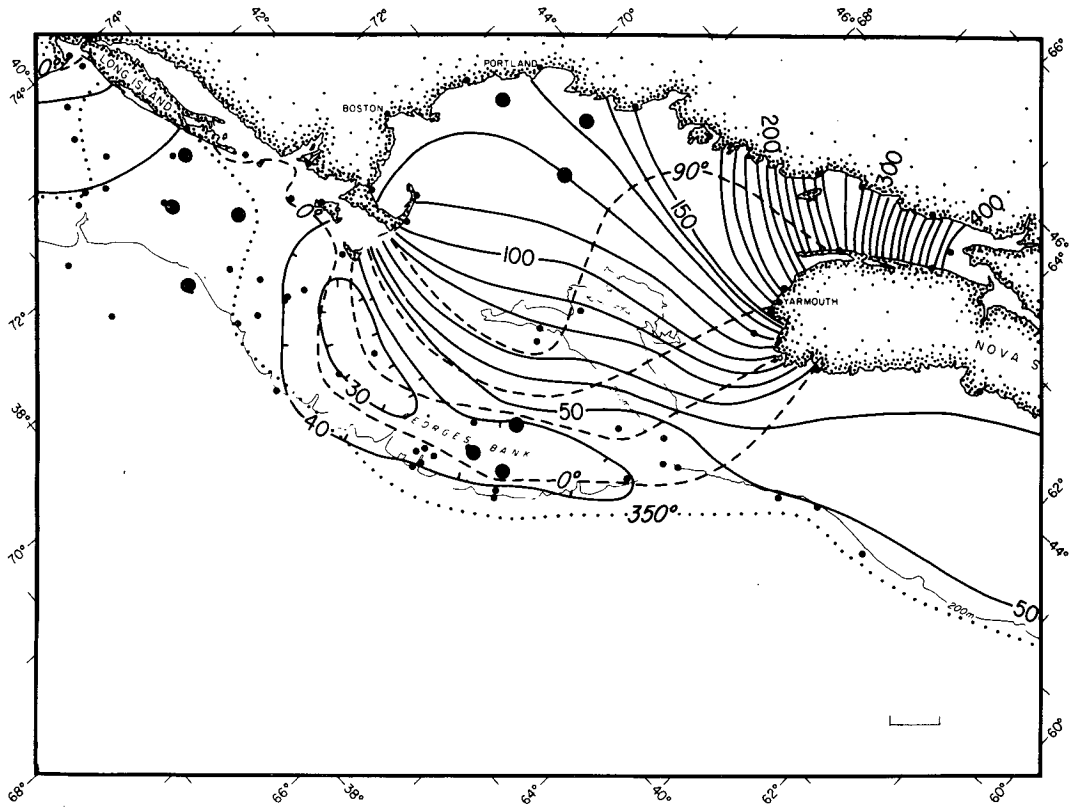

FIG. 2. An M_2 cotidal chart of the northeast continental shelf and Gulf of Maine which shows the near-resonance of the semidiurnal tide in the region. This picture has been constructed by Moody *et al.* (1983) from coastal and seafloor pressure (small dots) measurements. The local tidal dynamics of the three regions bracketed by the pressure stations identified with large dots are investigated in this paper.

$$\frac{\partial v}{\partial t} + \frac{\partial uv}{\partial x} + \frac{\partial v^2}{\partial y} + \frac{\partial vw}{\partial z} + fu = -\frac{1}{\rho}\frac{\partial \hat{p}}{\partial y} + \frac{1}{\rho}\left(\frac{\partial \tau_{xy}}{\partial x} + \frac{\partial \sigma_{yy}}{\partial y} + \frac{\partial \tau_{zy}}{\partial z}\right), \quad (4)$$

where $\hat{p}$ is pressure, ρ density, f the constant Coriolis parameter, and σ and τ are the normal and tangential stresses, respectively. (For horizontal scales to be considered here the gradient of the tide potential can be neglected).

For reasonably long waves at tidal and subtidal frequencies the vertical momentum equation reduces to the hydrostatic balance

$$\frac{\partial \hat{p}}{\partial z} = -\rho g,$$

which when integrated from an arbitrary level z to mean sea level at $z = 0$ leads to

$$\hat{p}(0) - \hat{p}(z) = -g\int_z^0 \rho dz. \quad (5)$$

The near-surface pressure $\hat{p}(0)$ can be written in terms of sea-level atmospheric pressure, p_a, and sea-level deviation, η, as

$$\hat{p}(0) = p_a + \rho_s g\eta, \quad (6)$$

where ρ_s is the near-surface density $\rho(0)$. If we partition the density field according to $\rho = \rho_0 + \rho'(x, y, z, t)$, where ρ_0 is a constant reference density and ρ' is the small departure from ρ_0, then (5) and (6) can be combined as

$$\hat{p}(z) = p_a + \rho_s g\eta - \rho_0 gz + g\int_z^0 \rho' dz. \quad (7a)$$

For dynamical considerations we need only consider deviations from the hydrostatic (i.e., motionless) state, so we define a perturbation pressure $p(x, y, z, t) = \hat{p}(x, y, z, t) + p_0 gz$ (remembering z is negative as defined here) and (7a) becomes

$$\frac{p(z)}{\rho_0} = \frac{p_a}{\rho_0} + \frac{\rho_s}{\rho_0} g\eta + \frac{g}{\rho_0}\int_z^0 \rho' dz. \quad (7b)$$

When the integrated density term (the only depth − dependent contribution to pressure) is evaluated for $z = -h$, then (7b) becomes a relation between perturbation bottom pressure and contributions from atmospheric pressure, sea level and integrated density perturbations. It can be shown that vertical integration of (3) and (4) combined with liberal use of Leibnitz's rule and the use of (2) and (7b) leads to the following vertically integrated form of the momentum equations,

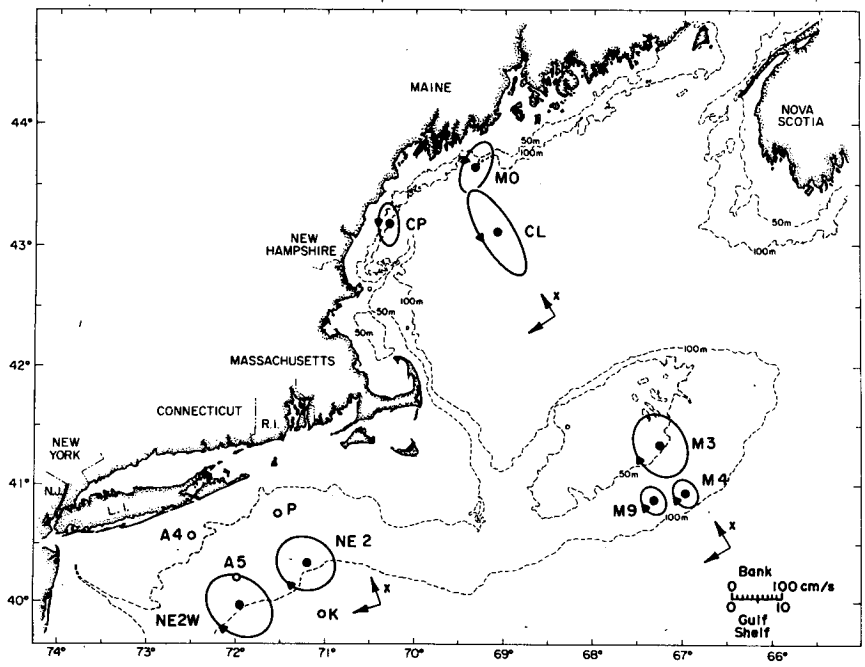

FIG. 3. Location of the stations used in the tidal dynamics study. Bottom pressure–current stations CL, CP and MO were part of a WHOI/University of New Hampshire (UNH) Gulf of Maine winter dynamics study; current stations NE2 and NE2W and bottom pressure stations P and K were part of a WHOI/UNH shelf dynamics study; bottom pressure stations A4 and A5 were part of a NOAA mid-Atlantic Bight study (MESA); and bottom pressure–current stations M3, M4, and M9 were part of a BLM-funded physical oceanographic study of Georges Bank. The M_2 tidal ellipses for vertically averaged currents are shown at the locations of currents used for this study. Note that the scale of the Georges Bank currents is 1/10 that of the others. The orientations of the across-isobath coordinate (X) for Georges Bank, the Gulf of Maine and the New England shelf are 332, 324 and 340°T, respectively.

$$\underset{\text{(a)}}{\frac{\partial \bar{u}}{\partial t}} + \underset{\text{(b)}}{\frac{\partial \overline{uu}}{\partial x}} + \underset{\text{(b)}}{\frac{\partial \overline{uv}}{\partial y}} - \underset{\text{(c)}}{f\bar{v}} = \underset{\text{(d)}}{-\frac{h}{\rho_0}\frac{\partial p_b}{\partial x}} + \underset{\text{(e)}}{\frac{g}{\rho_0}\frac{\partial [\psi]}{\partial x}} + \underset{\text{(f)}\quad\text{(g)}}{\frac{1}{\rho_0}[(\tau_x^{\,s} - \tau_x^{\,b}) + \alpha]}, \quad (8)$$

$$\underset{\text{(a)}}{\frac{\partial \bar{v}}{\partial t}} + \underset{\text{(b)}}{\frac{\partial \overline{uv}}{\partial x}} + \underset{\text{(b)}}{\frac{\partial \overline{vv}}{\partial y}} + \underset{\text{(c)}}{f\bar{u}} = \underset{\text{(d)}}{-\frac{h}{\rho_0}\frac{\partial p_b}{\partial y}} + \underset{\text{(e)}}{\frac{g}{\rho_0}\frac{\partial [\psi]}{\partial y}} + \underset{\text{(f)}\quad\text{(g)}}{\frac{1}{\rho_0}[(\tau_y^{\,s} - \tau_y^{\,b}) + \beta]}, \quad (9)$$

where again the overbar refers to the vertical integral as defined previously, τ^s and τ^b refer to surface and bottom stress, respectively, p_b is bottom pressure, and density contributions are contained in

$$\psi = \int_{-h}^{\eta}\int_{z}^{0} \rho'(\zeta)d\zeta dz - h\int_{-h}^{0}\rho'(z)dz$$

and lateral stress contributions are contained in

$$\alpha = \frac{\partial(hT_x)}{\partial x} + \frac{\partial(hT_x)}{\partial y}; \quad \beta = \frac{\partial(hT_y)}{\partial x} + \frac{\partial(hT_y)}{\partial y},$$

where T denotes vertically averaged stress. Terms (a), (b) and (c) of (8) and (9) are the vertically integrated versions of the inertial, nonlinear and Coriolis terms, respectively. The pressure gradient term is divided into the local perturbation bottom pressure gradient term (d) and the contribution due to internal density variability term (e). The stress term is divided into the difference between surface and bottom stress term (f) and the lateral gradients of the vertically averaged stress term (g).

We now assume that lateral gradients of stress components are much smaller than the vertical differences of horizontal stresses because the regions of interest here are well-removed from any coastal boundary layer. Then the horizontal integration of (8) and (9) over a rectangular area $A = \Delta y \Delta x = (y_2 - y_1)(x_2 - x_1)$ leads to the following area-averaged form of the momentum equations:

$$\frac{\rho_0}{A}\left\{\frac{\partial[u]}{\partial t}+\langle\delta_x\overline{uu}\rangle_y+\langle\delta_y\overline{uv}\rangle_x-f[v]+\frac{1}{\rho_0}\left\langle h\frac{\partial p_b}{\partial x}\right\rangle\right\}=\frac{\langle\tau_x^{\,s}-\tau_x^{\,b}\rangle}{A}+\frac{g}{A}\frac{\partial[\psi]}{\partial x}, \quad (10)$$

$$\frac{\rho_0}{A}\left\{\frac{\partial[v]}{\partial t}+\langle\delta_x\overline{uv}\rangle_y+\langle\delta_y\overline{vv}\rangle_x+f[u]+\frac{1}{\rho_0}\left\langle h\frac{\partial p_b}{\partial y}\right\rangle\right\}=\frac{\langle\tau_y^{\,s}-\tau_y^{\,b}\rangle}{A}+\frac{g}{A}\frac{\partial[\psi]}{\partial y}, \quad (11)$$

where the notation for the different integrals and differences are

$$\langle\ \rangle\equiv\int_{y_1}^{y_2}\int_{x_1}^{x_2}\cdots dxdy,$$

$$[\ ]\equiv\int_{y_1}^{y_2}\int_{x_1}^{x_2}\int_{-h}^{\eta}\cdots dzdxdy,$$

$$\langle\ \rangle_y\equiv\int_{y_1}^{y_2}\cdots dy,\quad\langle\ \rangle_x\equiv\int_{x_1}^{x_2}\cdots dx,$$

$$\delta_x f(x,y)=f(x_2)-f(x_1),\quad\text{and}$$

$$\delta_y f(x,y)=f(y_2)-f(y_1).$$

Equations (10) and (11) show that, if the pressure gradient contributions due to the density variability are insignificant, then, in principle, the surface–bottom stress difference can be inferred by computing the left-hand side (lhs) terms in the stress balance. The next section describes how observations of Georges Bank, Gulf of Maine and New England shelf tidal currents and pressures and (10) and (11) are used to explore dynamical balances and what uncertainties are associated with the process.

3. The M_2 semidiurnal tidal dynamic balances

Although the form of the momentum equations derived in the previous section is applicable over a wide range of frequencies the focus here will be on the M_2 semidiurnal tidal response of three different regions in question. Sets of moored bottom pressure and current observations made 1) on Georges Bank between 18 June and 15 August 1978 and described by EG&G (1979a,b,c and 1980), 2) in the western Gulf of Maine between 15 November 1974 and 15 January 1975 and described by Brown and Beardsley (1978) and Vermersch *et al.* (1979) and 3) on the New England shelf between 20 February and 15 August 1976 and described by Ou *et al.* (1980) were used for this study.

In order to extract the part of the original pressure and current time series observations that is coherent with the astronomy, a harmonic analysis of each time series was performed. The method used here is a modified form of the National Ocean Survey (NOS) harmonic analysis method (Dennis and Long, 1971), which analyzes directly for the M_2, N_2, S_2, O_1, K_1, M_4, M_6, M_8, S_4 and S_6 constituents and infers another 15 minor constituents using equilibrium tidal relationships. We have performed response analyses of some of these data and find that the NOS method is quite adequate for determining the M_2 semidiurnal constituent in these regions where the M_2 tidal response is clearly dominant. This is the case for the regions considered here as shown by the comparison of standard deviations of the observed series, the residual series (observed minus total predicted tides) and the M_2-tidal series in the right-hand columns of Tables A1 and A2 in Appendix A.

The quality of the M_2 semidiurnal tidal analysis is dictated in large part by the relative magnitude of the internal tide which is generally incoherent with the barotropic or external tide. On the southern flank of Georges Bank, Brown *et al.* (1982) have shown that the contributions due to the internal M_2 tides, which can contaminate the barotropic tidal current signal, are small. The western Gulf of Maine observations were made during the winter of 1974–75 when the water column was vertically well-mixed during most of the period (Brown and Beardsley, 1978) and therefore we conclude that the internal M_2 tides were not important in that case. Most of the nontidal variance found in the western Gulf of Maine is apparently due to subtidal-frequency mesoscale motion as discussed by Vermersch *et al.* (1979). On the New England shelf, the current harmonic analyses were performed only on the February through mid-May part of observations when hydrographic observations (Limeburner *et al.*, 1978) show that stratification was relatively weak and moored temperature spectra exhibit very little intensification at M_2 frequencies. Therefore we conclude that like the western Gulf the subtidal-frequency mesoscale features in the circulation are responsible for most of the nontidal variance in the observed currents. The overall evidence suggests that the internal semidiurnal tides are small in each of the regions of interest so that the harmonic analyses provide a reasonably accurate picture of the external tide.

Here we will focus on external M_2 tidal dynamics in each of the regions shown in Fig. 3 by predicting a 25-hour "noise-free" M_2-series corresponding to each observed series. The use of a monochromatic input series for these computations is allowed in this case because the nonlinear contributions to the local tidal momentum balance will be shown to be negligible. The currents in each region are rotated so that the coordinate system is generally across-isobath onshore and along-isobath towards the southwest in directions indicated in Table A2 of Appendix A. The details of the computation for each region will be treated separately as follows.

a. Georges Bank

Of the three regions considered here the southern flank of Georges Bank (the Bank henceforth) is most clearly dominated by the external semidiurnal (M_2) tide. The tidal sea level amplitudes are similar to those over adjacent continental shelf regions, while the tidal currents are much larger than over adjacent regions because of the amplified tidal transport associated with the near-resonant response of the Gulf of Maine. The current components have been computed for across-isobath (X) and along-isobath (Y) directions of 330 and 240°T respectively which are approximately aligned with the directions of the major and minor axes of the vertically-averaged M_2-tidal-current ellipse (see Fig. 3), with $+z$ upwards. The velocity components in this rotated coordinate system are computed at each level where measurements are available and are used to compute estimates of the vertical integral of current (indicated by an overbar) as summarized in Appendix B. The amplitudes of station M3 and M9 currents, which were observed only at 8 and 6 m above the bottom, respectively, have been amplified in accordance with the ratios of tidal currents observed at different depths by Moody and Butman (1980) at locations near these sites respectively. In addition, the station M9 currents have been lagged by 1 hour[1] to account for the phase shift that exists between the near-bottom and vertically averaged tidal currents in the Moody and Butman (1980) observations. The M_2 harmonic constants of the depth-averaged currents in this study are presented in Table 1.

A summary of how momentum-related terms are estimated from the vertically integrated currents at individual stations is presented in Table 2, in which the assumption used making each estimate appears to the right. The inertial term is computed from a time-centered two-hour first difference of the integrated velocity and amplified by 4.2% to account for the systematic underestimate of its amplitude as discussed in Appendix C. Then all terms on the lhs of (10) and (11) are computed by multiplying the results of Table 2 by the appropriate constants. After the estimates of individual terms (in stress units of dyn cm^{-2}) have been computed, the *negative sum* of these lhs terms or "residual" is formed. The residual contains contributions from the horizontal stress difference, $\tau^s - \tau^b$, any density-related effects which are coherent with the astronomical tide, and uncertainties associated with this computation.

Time series of the instantaneous along- and across-isobath "stress balances" for the Bank are shown in Fig. 4 while the corresponding standard deviations of the individual terms (computed for a semidiurnal period) are presented in Table 3. It can be seen that in the across-isobath direction a sum of the Coriolis and pressure gradient terms nearly balances the larger inertial acceleration term, while in the along-isobath direction, there is a near-balance between the inertial and Coriolis terms. Both the residual and the nonlinear term estimates are clearly smaller than the principal dynamical elements whose configuration is consistent with local progressive-wave dynamics. We shall return to this point later.

The usefulness of these preliminary conclusions regarding dynamical balances depends upon the magnitude of the computational uncertainties that have been estimated. (Because of the dominance of the M_2 response at these sites these uncertainty estimates should apply to the total signal as well). The uncertainty considerations, which are outlined in Appendix C, attempt to account for the propagation of errors associated with uncertainties in the original data series *plus* uncertainties associated with making estimates of integral and differential terms as outlined in Table 2. The results of the uncertainty analysis, which are indicated in Table 3, show that the principal terms in the dynamical balances are estimated well. At first glance it would seem that the bottom stress (which is not estimated directly) could be inferred from the residual term. However our uncertainty analysis suggests that that is difficult as will be discussed later.

b. Gulf of Maine

The near-resonance of the Gulf of Maine–Bay of Fundy basin at semidiurnal frequencies leads to the amplified sea levels observed at the western Gulf location (see Appendix A, Table A1). On the other hand in contrast to the Bank, the Gulf M_2 currents are relatively modest (see Appendix A, Table A2). For this tidal dynamics analysis all currents were rotated according to a single set of across- and along-isobath directions of 324 (X) and 234°T (Y), respectively.

The vertical integrals of currents at the Monhegan (MO) and Cashes Ledge (CL) moorings were computed according to Simpson's rule (see Appendix B). The single 33-m current at Cape Porpoise (CP) has been amplified and lagged in accordance with the ratio and phase between the 33-m and vertically averaged currents at Monhegan (MO). In Table 2 we present a summary of how momentum-related term estimates are formed from the vertically integrated currents from the individual stations.

The details of the instantaneous stress balance for the Gulf are compared with balances from the Bank and the Shelf in Fig. 4 and in Table 3. In the across-isobath direction a sum of the inertial and Coriolis terms (and residual) balances the relatively large pressure gradient term while in the along-isobath direction the same balance exists, but here a relatively large residual term assists the pressure gradient in balancing

[1] Although this might be ½ hour too large according to B. Butman (personal communication, 1983), we find the results are relatively insensitive to uncertainties of this magnitude.

TABLE 1. A summary of M_2 tidal harmonic constants for observed bottom pressures and depth averaged currents, computed volume averaged currents (VOL) for all three regions and Greenberg's (1983) numerical model pressure-equivalent sea levels and currents from the Bank and Gulf (presented in parentheses). The harmonic constants are presented in terms of pressure (H), across-isobath (u_0) and along-isobath (v_0) current amplitudes [in units of millibars (mb) and cm s^{-1}] and Greenwich phases G. The ellipse characteristics of the currents are presented in terms of major- and minor-axis amplitudes, Greenwich phase (G) and orientation ϕ (in °T), of the major-axis current and ellipticity e = −major/minor. The model-current components have been realigned with the observed coordinate systems which are 330°T(X)/240°T(Y) for Georges Bank, 324°T(X)/234°T(Y) for the Gulf of Maine and 340°T(X) and 250°T(Y) for the New England shelf.

Site	Station	Latitude Longitude	Bottom pressure		Across-isobath		Along-isobath		Current ellipse				
			H	G	u_0	G_u	v_0	G_v	major	minor	G	ϕ(°T)	e
Georges Bank	M3	41°19.8′ 67°15.0′	39.6 (36)	22 (23)	64.6 (58.5)	2 (9)	50.1 (50.0)	272 (267)	64.6 (61.1)	50.1 (46.9)	2 (30)	330 (356)	−1.29 (−1.17)
	M4	40°55.2′ 66°58.2′	38.5 (40)	1 (0)	33.6 (26.9)	14 (6)	22.2 (21.1)	287 (280)	33.6 (27.0)	22.1 (20.9)	12 (0)	327 (322)	−1.52 (−1.27)
	M9	40°53.4′ 67°23.4′	38.9 (40)	6 (6)	37.6 (33.1)	21 (3)	23.0 (24.8)	280 (274)	38.0 (33.1)	22.4 (24.8)	27 (2)	340 (329)	−1.69 (−1.33)
	VOL	41°07.0′ 67°19.5′	—	—	45.4 (40.2)	10 (7)	32.2 (32.6)	277 (271)	45.5 (40.6)	32.1 (32.1)	13 (16)	332 (342)	−1.43 (−1.26)
Gulf of Maine	CP	43°13.2′ 70°16.8′	127.8 (136)	103 (105)	3.5 (6)	6 (352)	2.8 (3)	131 (120)	4.0 (6.7)	2.0 (2.8)	348 (340)	358 (353)	2.00 (2.39)
	MO	42°40.2′ 69°22.8′	131.3 (139)	99 (100)	3.8 (6)	36 (21)	5.2 (5)	163 (143)	5.8 (7.3)	2.7 (4.4)	359 (352)	23 (9)	2.15 (1.66)
	CL	43°10.8′ 69°04.8′	120.7 (127)	98 (99)	10.1 (13)	17 (13)	4.2 (5)	117 (139)	10.1 (14.2)	4.1 (4.6)	15 (14)	329 (333)	2.46 (3.09)
	VOL	43°12.0′ 69°40.8′	—	—	7.9	18	3.9	128	8.0	3.6	12	336	2.22
New England shelf	NE2	40°21.7′ 71°12.0′	—	—	6.2	304	5.9	219	6.3	5.7	275	309	−1.11
	NE2W	39°58.9′ 71°57.4′	—	—	8.0	273	6.2	209	8.7	5.2	254	310	−1.67
	A4	40°34.2′ 72°18.0′	48.3	346	—	—	—	—	—	—	—	—	—
	A5	40°11.4′ 72°00.0′	47.0	349	—	—	—	—	—	—	—	—	—
	P	40°43.2′ 71°19.2′	43.5	348	—	—	—	—	—	—	—	—	—
	K	39°55.8′ 71°03.0′	42.5	347	—	—	—	—	—	—	—	—	—
	VOL	40°18.0′ 71°34.8′	—	—	7.1	286	6.2	214	7.7	5.5	82	307	−1.40

the results. As with the Bank computation the Gulf nonlinear terms are negligible.

The residual in this case must be composed principally of computational uncertainties because the currents and thus bottom stresses are relatively small. In particular the estimate of the along-isobath pressure gradient, which is the most uncertain anyway (see Appendix C), is represented by observations on the most shoreward edge of the area and may contribute to the larger uncertainty of this computation. Thus we conclude that the principal dynamical balance in the Gulf is between the pressure gradient term and a sum of the inertial and Coriolis terms. In contrast to the progressive wave dynamics of the Bank these results suggest that frictionless standing wave dynamics are a better approximation to western Gulf tidal dynamics.

c. *New England shelf*

The New England shelf region south of Rhode Island is characterized by modest tidal elevations and currents, when compared to the Gulf elevations and the Bank

TABLE 2. A summary of the approximations and corresponding assumptions used to estimate the terms in the volume integrated momentum equations for Georges Bank, the Gulf of Maine and the New England shelf. Subscripts refer to the stations shown in Fig. 3.

Site	Term	Estimate	Assumptions
Georges Bank	$[u]$	$\{(\bar{u}_{M4} + \bar{u}_{M3})0.5 + \bar{u}_{M9}\}(0.5\Delta x\Delta y)$	linear velocity variation
Δx = 43 km	$[v]$	$\{(\bar{v}_{M4} + \bar{v}_{M3})0.5 + \bar{v}_{M9}\}(0.5\Delta x\Delta y)$	linear velocity variation
Δy = 33 km	$\langle\delta_x\overline{uu}\rangle_y$	$[(\bar{u}_{M3}\bar{u}_{M3}/h_{M3}) - (\bar{u}_{M4}\bar{u}_{M4}/h_{M4})]\Delta y$	no y-variation in $\delta_x\overline{uu}$
	$\langle\delta_x\overline{uv}\rangle_y$	$[(\bar{u}_{M3}\bar{v}_{M3}/h_{M3}) - (\bar{u}_{M4}\bar{v}_{M4}/h_{M4})]\Delta y$	no y-variation in $\delta_x\overline{uv}$
	$\langle\delta_y\overline{uv}\rangle_x$	$[(\bar{u}_{M9}\bar{v}_{M9}/h_{M9}) - (\bar{u}_{M4}\bar{v}_{M4}/h_{M4})]\Delta x$	no x-variation in $\delta_y\overline{uv}$
	$\langle\delta_y\overline{vv}\rangle_x$	$[(\bar{v}_{M9}\bar{v}_{M9}/h_{M9}) - (\bar{v}_{M4}\bar{v}_{M4}/h_{M4})]\Delta x$	no x-variation in $\delta_y\overline{vv}$
	$\langle h\partial p_b/\partial x\rangle$	$[(h_{M3} + h_{M4})0.5][p_{M3} - (p_{M4} + p_{M9})0.5]\Delta y$	$\partial p_b/\partial x$ constant on A
	$\langle h\partial p_b/\partial y\rangle$	$[(h_{M3} + h_{M4})0.5][p_{M9} - p_{M4}]\Delta x$	$\partial p_b/\partial y$ constant on A
Gulf of Maine	$[u]$	$\{(\bar{u}_{MO} + \bar{u}_{CP})0.5 + \bar{u}_{CL}\}(0.5\Delta x\Delta y)$	Same as for Georges Bank
Δx = 59 km	$[v]$	$\{(\bar{v}_{MO} + \bar{v}_{CP})0.5 + \bar{v}_{CL}\}(0.5\Delta x\Delta y)$	
Δy = 87 km	$\langle\delta_x\overline{uu}\rangle_y$	$[(\bar{u}_{CL}\bar{u}_{CL}/h_{CL}) - (\bar{u}_{MO}\bar{u}_{MO}/h_{MO})]\Delta y$	
	$\langle\delta_x\overline{uv}\rangle_y$	$[(\bar{u}_{CL}\bar{v}_{CL}/h_{CL}) - (\bar{u}_{MO}\bar{v}_{MO}/h_{MO})]\Delta y$	
	$\langle\delta_y\overline{uv}\rangle_x$	$[(\bar{u}_{CP}\bar{v}_{CP}/h_{CP}) - (\bar{u}_{MO}\bar{v}_{MO}/h_{MO})]\Delta x$	
	$\langle\delta_y\overline{vv}\rangle_x$	$[(\bar{v}_{CP}\bar{v}_{CP}/h_{CP}) - (\bar{v}_{MO}\bar{v}_{MO}/h_{MO})]\Delta x$	
	$\langle h\partial p_b/\partial x\rangle$	$[(h_{MO} + h_{CL})0.5](p_{MO} - p_{CL})\Delta y$	
	$\langle h\partial p_b/\partial y\rangle$	$[(h_{MO} + h_{CL})0.5](p_{CP} - p_{MO})\Delta x$	
New England shelf	$[u]$	$(\bar{u}_{NE2} + \bar{u}_{NE2W})(0.5\Delta x\Delta y)$	Same as for Georges Bank
Δx = 55 km	$[v]$	$(\bar{v}_{NE2} + \bar{v}_{NE2W})(0.5\Delta x\Delta y)$	
Δy = 80 km	$\langle\delta_y\overline{uv}\rangle_x$	$[(\bar{u}_{NE2W}\bar{v}_{NE2W}/h_{NE2W}) - (\bar{u}_{NE2}\bar{v}_{NE2}/h_{NE2})]\Delta x$	
	$\langle\delta_y\overline{vv}\rangle_x$	$[(\bar{v}_{NE2W}\bar{v}_{NE2W}/h_{NE2W}) - (\bar{v}_{NE2}\bar{v}_{NE2}/h_{NE2})]\Delta x$	
	$\langle h\partial p_b/\partial x\rangle$	$h_{NE2}[p_P - (0.625p_K + 0.375p_P)]\Delta y$	

currents (see Appendix A). For this tidal dynamics analysis all currents were rotated according to a single set of across- and along-isobath directions of 340 (X) and 250°T (Y) respectively.

For this region currents were available from stations NE2 and NE2W on the 83-m isobath, while bottom pressures were available from A4, A5, P and K. We found no significant difference between the tidal analysis of the 38 m currents and a vertical average of the 38 m and 73 m currents at NE2: a result that suggests that friction has a less important influence on the current profiles in the region. Thus the vertically integrated currents were estimated using only the 38 m currents as shown in Appendix B. As with the other analyses we present a summary of how the terms are estimated in Table 2. The nonlinear terms requiring estimates of across-isobath current gradients are not possible to compute on the Shelf but we expect that they are negligible here as at the other locations.

A comparison of the details of the instantaneous stress balances in Fig. 4 shows that the Shelf tidal dynamics are most similar to the Bank tidal dynamics. Although the amplitude ratio of the uncertainties to term estimates is relatively large compared to corresponding ratios on the Bank, the apparent first-order across-isobath and along-isobath balances are between the inertial term and a sum of the pressure gradient and Coriolis term. The along-isobath result contrasts with the Bank's near-balance between the inertial and Coriolis terms alone and is due to the relatively important along-isobath pressure gradients which are probably caused by the regional bend in the coastal configuration.

Thus we find distinctively different M_2 tidal dynamics on the Georges Bank and in the Gulf of Maine, with the results for the New England shelf being less easily categorized. On the Bank a progressive wave is forced by oceanic-induced across-isobath pressure gradient which works in concert with the Coriolis force to produce a clockwise (*cum sole*) rotating current. The magnitude of the current is relatively large because of the mass flux requirements of a near-resonant Gulf semidiurnal tidal response. In the Gulf of Maine a standing wave is characterized by a relatively small counterclockwise (*contra sole*) rotating tidal current which results from the difference between the dominant pressure gradient forces and the Coriolis forces. The relationships between a volume-averaged flow and pressure gradient forces are contrasted for the Bank and Gulf in Fig. 5.

4. Discussion

a. Local M_2 semidiurnal tidal dynamics

As we can see in Fig. 2 the three sets of observations are located in very different tidal regimes. The Georges

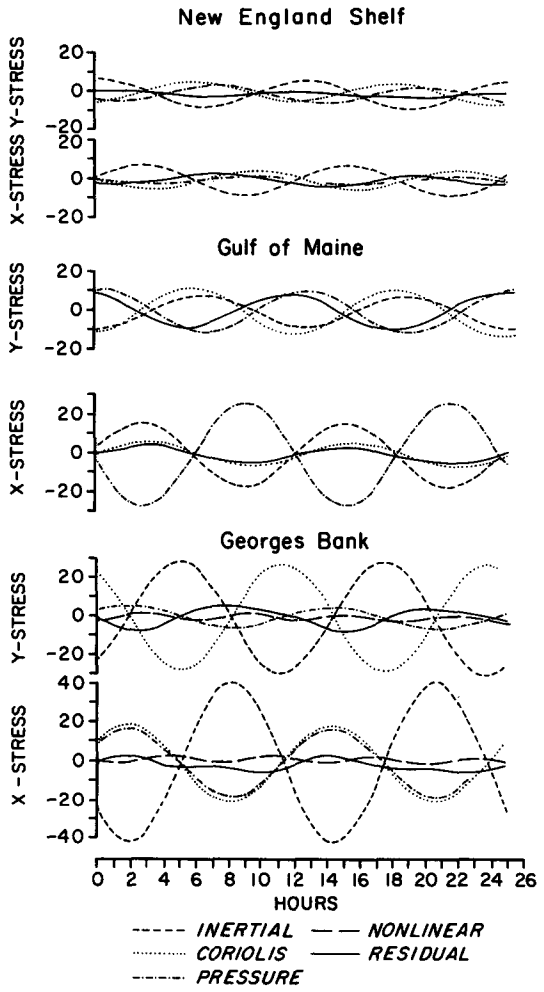

FIG. 4. A comparison of terms in the along- and across-isobath stress-balance for the M_2-series input from (a) Georges Bank, (b) Gulf of Maine and (c) the New England shelf. The stress units are in dyn cm^{-2} and the abscissa values are in hours relative to 0000 GMT 19 June 1978, 21 November 1974 and 26 March 1976 for (a), (b) and (c) respectively.

Bank array is located in a region where the M_2 tidal wave is propagating across-isobath with little local amplitude attenuation or amplification. The Gulf of Maine array is located in a region, which exhibits standing wave characteristics with small phase changes and some amplitude amplification shoreward. The New England Shelf array is located in a more confused transition region which exhibits both small phase changes and amplitude changes across the array. With these preliminary observations in mind we seek to relate the dynamical balances we have found in the previous section for the different regions to simple dynamical models of waves at the semidiurnal tidal frequency.

For Georges Bank the first-order dynamic balances are the same as those for a long gravitational gyroscopic wave propagating in the x-direction through a constant-depth frictionless ocean. The dynamics of the progressive form of this wave, more commonly called a Sverdrup wave, can be expressed in terms of the appropriate continuity equation

$$\frac{\partial \eta}{\partial t} + h\frac{\partial u}{\partial x} = 0 \tag{12}$$

and the two momentum equations

$$\frac{\partial u}{\partial t} = -g\frac{\partial \eta}{\partial x} + fv, \tag{13}$$

$$\frac{\partial v}{\partial t} = -fu, \tag{14}$$

where η is the free surface perturbation, u and v the depth-averaged velocities in the direction of and normal to the propagation direction respectively, h the depth and g the gravitational acceleration. A solution to these equations for a positive x propagating wave of the form $\eta = \eta_0 \cos(\omega t - kx)$ is

$$\left.\begin{aligned} u &= \left\{\left[\frac{g}{h}\right]\left[1 - \left(\frac{f}{\omega}\right)^2\right]\right\}^{1/2} \eta_0 \cos(\omega t - kx) \\ v &= -\left\{\left[g\left(\frac{f}{\omega}\right)^2 h^{-1}\right]\left[1 - \left(\frac{f}{\omega}\right)^2\right]\right\}^{1/2} \eta_0 \sin(\omega t - kx) \end{aligned}\right\},$$

TABLE 3. A comparison of the semidiurnal period standard deviations of stress balance terms (in units of dyn cm^2) for the across- and along-isobath computations for Georges Bank, the Gulf of Maine and the New England shelf. A discussion of uncertainty estimates appears in Appendix C. The results from an identical computation, using Greenberg's (1983) numerical model currents and pressures from the appropriate Georges Bank locations, are presented in parentheses for comparison.

Term	Georges Bank	Gulf of Maine	New England
Across-isobath			
Inertial $\frac{\rho_0}{A}\frac{\partial [u]}{\partial t}$	29.8 ± 2.6 (26.3)	10.9 ± 1.2	5.2 ± 0.7
Nonlinear $\frac{\rho_0}{A}\langle \delta_x \overline{uu} \rangle_y$	1.0 ± 1.3 (0.9)	0.1 ± 0.1	—
Nonlinear $\frac{\rho_0}{A}\langle \delta_y \overline{uv} \rangle_x$	0.1 ± 0.4 (0.3)	0.0 ± 0.0	0.0 ± 0.0
Coriolis $\frac{\rho_0}{A} f[v]$	14.4 ± 1.3 (14.5)	4.0 ± 0.4	3.5 ± 0.5
Pressure gradient $\frac{1}{A}\langle h\frac{\partial p_b}{\partial x}\rangle$	13.2 ± 1.2 (14.6)	18.6 ± 2.9	1.1 ± 0.9
Residual	2.6 ± 3.4 (4.8)	4.1 ± 3.2	2.1 ± 1.3
Along-isobath			
Inertial $\frac{\rho_0}{A}\frac{\partial [v]}{\partial t}$	21.2 ± 1.8 (21.3)	5.7 ± 0.6	5.2 ± 0.6
Nonlinear $\frac{\rho_0}{A}\langle \delta_x \overline{uv} \rangle_y$	0.9 ± 1.1 (0.7)	0.0 ± 0.0	—
Nonlinear $\frac{\rho_0}{A}\langle \delta_y \overline{vv} \rangle_x$	0.1 ± 0.2 (0.2)	0.0 ± 0.0	0.0 ± 0.0
Coriolis $\frac{\rho_0}{A} f[u]$	20.3 ± 1.7 (17.9)	8.4 ± 0.9	3.7 ± 0.5
Pressure gradient $\frac{1}{A}\langle h\frac{\partial p_b}{\partial y}\rangle$	4.7 ± 1.5 (5.8)	8.0 ± 2.0	2.9 ± 0.7
Residual	5.6 ± 3.2 (8.4)	6.5 ± 2.3	1.0 ± 1.0

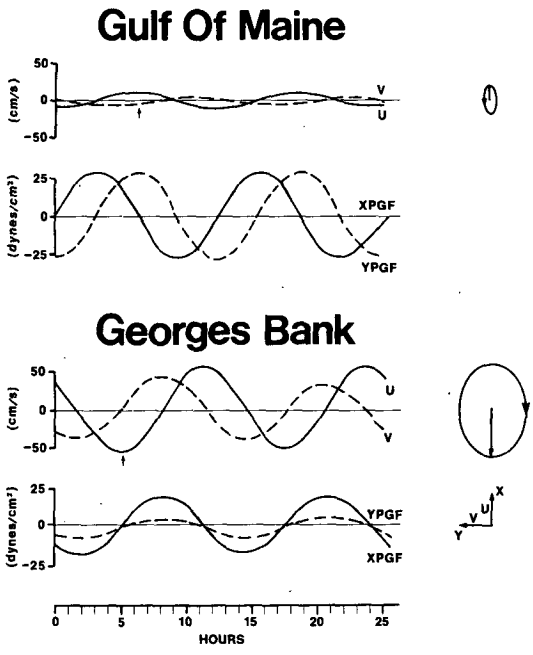

FIG. 5. The relationship between the across- and along-isobath pressure gradient forces (*XPGF*, *YPGF*) and the volume averaged flow components (*U*, *V*) which form the tidal elliptical motion on Georges Bank and in the Gulf of Maine. The initial phase is indicated by the arrow and the vector in the ellipse. The Gulf *YPGF* is amplified in order to account for our underestimate of it (see text Section 3c).

where ω is the specified frequency which is greater than the inertial frequency, f, k is the wavenumber and the phase speed is $\omega/k = [\omega/(\omega^2 - f^2)^{1/2}](gh)^{1/2}$. An additional characteristic of interest is the ellipticity, defined here as $e = iu/v$ and is $-\omega/f$, where the negative sign in this case refers to a clockwise rotation of the velocity vector. The relationship between forces and flow accelerations in a Sverdrup wave are shown in Fig. 6 for a wave period.

Given the observed equivalent sea-level perturbation amplitude $\eta_0 = 39$ cm and the mean depth $\bar{h} = 60.5$ m for the Georges Bank region, the Sverdrup wave M_2 velocity amplitudes are

$$\left.\begin{aligned} u_0 &= \left\{\left[\frac{g}{h}\right]\left[1 - \left(\frac{f}{\omega}\right)^2\right]\right\}^{1/2} \eta_0 \\ v_0 &= \left\{\left[g\left(\frac{f}{\omega}\right)^2 h^{-1}\right]\left[1 - \left(\frac{f}{\omega}\right)^2\right]\right\}^{1/2} \eta_0 \end{aligned}\right\},$$

respectively, have been computed and are compared with observations in Table 4. Although the theoretical ellipticity in this case is very near the observed Sverdrup wave ellipticity, the Sverdrup velocities are considerably less than the observed velocities and the simple model fails to describe the quantitative features of the observed results.

Even when applied locally at stations M3, M4 and M9, as presented in Table 4, the Sverdrup wave model fails to explain the relationships between velocity and amplitudes because the Sverdrup wave pressure gradient is much smaller than that observed. However this lack of quantitative agreement between observations and simple Sverdrup wave dynamics is probably not surprising since the Bank water depth changes from about 78 to 44 m (or 56% of the mean depth) across the array (see Fig. 7). In addition, though not of first-order significance, friction is important enough to influence the flow profiles as discussed in Section 6 and may be important enough to consider.

The difficulty is addressed here by noting that although there is some along-isobath (Y) variability in the across-isobath (X) transport, as shown in the Table 4 comparison of M4 and M9 transports, the average of the two numbers is 28.5 $m^2 s^{-1}$ and nearly the same as that found at M3 and that computed for the volume-averaged dynamics. Thus we assume, as Loder (1980) did in his two-dimensional study of tidal current rec-

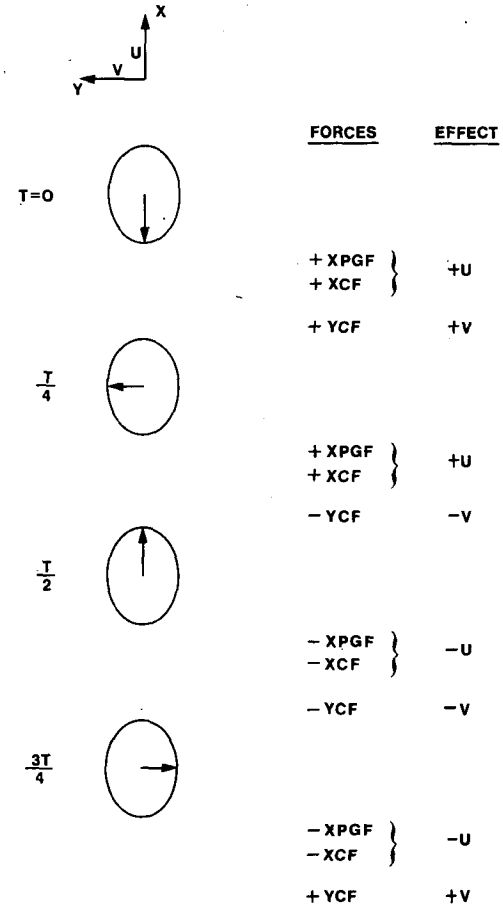

FIG. 6. The Sverdrup wave relationship between the across-isobath pressure gradient force (*XPGF*), across- and along-isobath Coriolis forces (*XCF*, *YCF*) and tidal ellipse motion. The initial wave phase at $T = 0$ (shown to the left) is chosen to coincide with minimum u. The forces, which act on the flow during succeeding quarter tidal periods, are shown with their effects on the flow components to the right. Here *XPGF* and *XCF* combine to accelerate the u velocity, while the *YCF* steers the flow through its clockwise elliptical path.

TABLE 4. A comparison of the observed, forced and Sverdrup wave velocity characteristics (u_0, v_0) which were computed assuming the observed tidal amplitude η_0 and depth H for the volume-averaged dynamics computation and at each of the observation stations. The following values for the M_2 tidal frequency ($\omega_{M2} = 1.405 \times 10^{-4}$ s^{-1}), the local inertial frequency ($f_{41°N} = 0.954 \times 10^{-4}$ s^{-1}) and gravitational acceleration ($g = 9.8$ m s^{-2}) have been used for these computations. The ellipticity e, for which positive values mean counterclockwise, and the across-isobath transport u_0H are also presented.

	H (m)	η_0 (m)	u_0 (m s^{-1})	v_0 (m s^{-1})	e	u_0H (m^2 s^{-1})
Volume-averaged						
Observed	62	0.390	0.454	0.322	−1.41	28.1
Forced			0.463	0.315	−1.47	28.0
Sverdrup			0.214	0.145	−1.47	12.9
M3						
Observed	44	0.396	0.646	0.501	−1.29	28.4
Forced			0.636	0.432	−1.47	28.0
Sverdrup			0.255	0.173	−1.47	11.2
M4						
Observed	79	0.385	0.336	0.222	−1.51	26.5
Forced			0.364	0.247	−1.47	28.0
Sverdrup			0.187	0.127	−1.47	14.4
M9						
Observed	81	0.389	0.376	0.230	−1.63	30.5
Forced			0.354	0.241	−1.47	28.0
Sverdrup			0.186	0.127	−1.47	14.7

tification on a bank, that the deep-ocean forced across-isobath transport on this part of Georges Bank is constant. Contrary to Loder's (1980) treatment, the small observed across-isobath phase progression will be incorporated also.

Water depth changes across-bank will be modeled according to $H(x) = h_{M4} - \alpha x$, where the x-origin is at station M4 (see Fig. 7) and the bottom slope is $\alpha = (h_{M4} - h_{M3})/a$ with the M4-to-M3 station separation, $a = 53$ km. Thus the across-isobath vertically averaged velocity can be written in terms of the constant transport T_0 as follows

$$u(x, t) = \left(\frac{T_0}{H(x)}\right) e^{i(\omega t - kx)} = U_0(x) e^{i(\omega t - kx)}, \quad (15)$$

where k is the local wavenumber.

With the additional assumption that the along-isobath depth-averaged current v and the sea level perturbation η have forms like u, then the x-dependent complex amplitudes $V_0(x)$ and $\eta_0(x)$ can be determined upon substitution of u into the momentum equations (13) and (14). From (14)

$$V_0 = i \frac{f}{\omega} U_0 \quad (16)$$

so that the current ellipticity is

$$e = -i \frac{u}{v} = -\frac{\omega}{f}, \quad (17)$$

or just as we found with Sverdrup waves. This result is the same in both linear, frictionless cases because the along-isobath pressure gradient is assumed to be negligible in both cases. Upon substitution of (15) and (16) into (13) we can find the pressure gradient amplitude $\eta_{x0} = (d\eta_0/dx - ik\eta_0)$ as

$$\eta_{x0} = -i \frac{(\omega^2 - f^2)}{g\omega} U_0 = -i \frac{\beta}{(h_{M4} - \alpha x)}. \quad (18)$$

The solutions that result are

$$\left.\begin{aligned} u &= U_0(x) \cos(\omega t - kx) \\ v &= -(f/\omega) U_0(x) \sin(\omega t - kx) \\ \eta_x &= \frac{\beta}{(h_{M4} - x)} \sin(\omega t - kx) \end{aligned}\right\}, \quad (19)$$

where $\partial/\partial x$ is denoted with the subscript x. The ratio of the pressure gradient and inertial forces is in this case

$$\frac{-g\eta_x}{u_t} = \frac{\omega^2 - f^2}{\omega^2},$$

which shows that the model phase agrees with observations.

Since the across-isobath transport has been chosen to force the wave the comparison of forced wave and observed across-isobath current results is, as expected, very good. The forced wave and observed along-isobath current comparison is also very good because the observed current components are so nearly described by (17). The question is how well do the model and observed across-isobath pressure gradient amplitudes compare?

If we incorporate the fact that kx is small (using the observed phase changes and distances it is found that $0 \leq kx \leq 0.25$), then

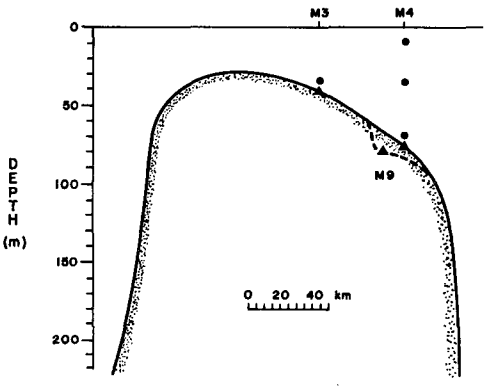

FIG. 7. A Georges Bank bathymetry transect (330°T) through moorings M3 and M4. An indication of the local bathymetry around mooring M9, which is downshelf from the line of the main transect, is shown along with the location of the bottom pressure and current meter instruments.

$$\eta_x \sim \frac{\beta}{(h_{M4} - \alpha x)} (\sin\omega t - kx \cos\omega t)$$

and the spatial average of the pressure gradient $\Delta\eta/a$ can be computed according to

$$\frac{\Delta\eta}{a} = \frac{1}{a}\int_0^a \eta_x dx = -\frac{\beta \sin\omega t}{\alpha a}[\ln(h_{M4} - \alpha x)]_0^a$$

$$-\frac{\beta k \cos\omega t}{\alpha^2 a}[(h_{M4} - \alpha x) - h_{M4}\ln(h_{M4} - \alpha x)]_0^a.$$

For the assumed transport, geometry, latitude and Coriolis parameter

$$\frac{\Delta\eta}{a} = \frac{\beta}{\alpha a}(-0.56 \sin\omega t - 0.09 \cos\omega t),$$

which has an rms value of 2.6×10^{-6}. Although this overestimates the observed rms pressure gradient amplitude of $1.8 \times 10^{-6} \pm 10\%$ by 36% the overly simplified forced wave model appears to contain the essential first-order physics of this forced tidal regime.

In summary, the above results suggest that the Georges Bank M_2 tides in the region of interest can be described in terms of a progressive wave, which is forced by the deep ocean tides and is characterized by nearly constant across-isobath transport and sea level amplitudes in the depth range between 80 and 44 m. Because the along-isobath pressure gradients, due to along-isobath irregularities, are locally small, the value of current ellipticities e are close to those of a Sverdrup wave (i.e., $e = -1.47$). A simple two-dimensional forced wave model, which includes a linear depth change and rotation, accounts for the current amplitudes very well and, although it overestimates space-averaged pressure gradients by 35%, appears to contain the principal physics governing the relationship of currents and pressure gradients.

With the kinematic pictures in the Georges Bank and Gulf of Maine being so different, it is not surprising that the tidal dynamical pictures in the two regions are so distinctly different. A summary of the relationship between forces and accelerations for Gulf of Maine counterclockwise rotary current motion, which has been inferred from the volume-integrated results and is shown in Fig. 8, is consistent with rotary standing-wave dynamics. Although the geometrical differences are substantial, there are striking qualitative similarities between the western Gulf of Maine tidal-ellipse distribution in Fig. 3 and Taylor's (1920) result (Fig. 9) for a reflected Kelvin wave in the end of a basin. In particular the tendency of the counterclockwise rotary current ellipses to align themselves with the coast at the more coastward stations is reproduced although the Gulf of Maine bathymetric effects obviously complicate the quantitative picture of current-ellipse characteristics. The sense of the pressure gradients and their relationship to the currents appear to be qualitatively similar in the two situations, thus providing convincing evidence of the relative importance of reflected Kelvin wave dynamics. Because the real Gulf of Maine dynamics must be complicated by the presence of Poincaré waves, which can be scattered from coastline and bottom irregularities as discussed by Mysak and Tang (1974) and May (1979), a quantitative treatment of this problem will not be attempted here. However, any future treatment of the details of the western Gulf of Maine tidal dynamics can probably neglect the effects of bottom friction (in contrast to Georges Bank), which is small because of the small current amplitudes.

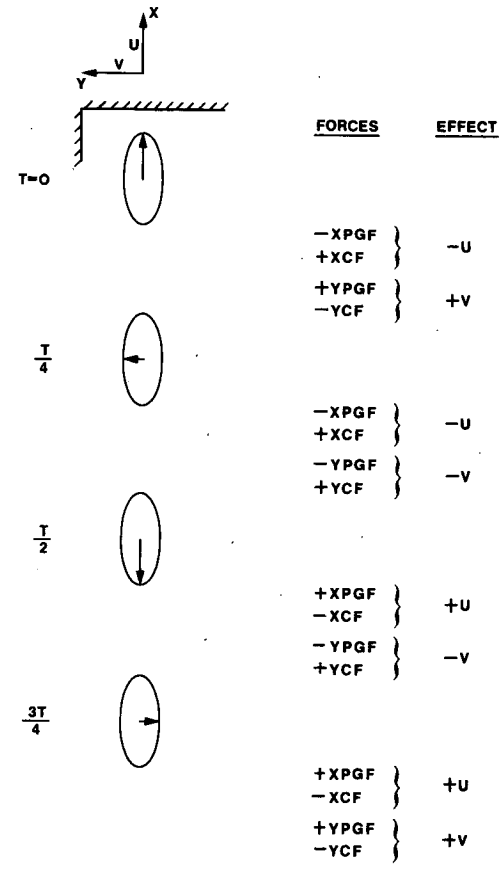

FIG. 8. The rotary standing wave relationship between across- and along-isobath pressure gradient forces (*XPGF, YPGF*), Coriolis forces (*XCF, YCF*) and the tidal ellipse motion. The initial wave phase at $T = 0$ (shown to the left) is chosen to coincide with the maximum u. The forces, which act on the flow during succeeding quarter tidal periods are shown with their effects on the flow components to the right. In this case pressure gradient forces, caused by the presence of nearby boundaries, overcome the effects of Coriolis forces to steer the flow through its counterclockwise elliptical path.

The tidal dynamics in our study region on the New England shelf are less easily explained than those found on either Georges Bank or on the New Jersey shelf to the southwest because the alongshelf tidal pressure gradient (a) is relatively more important in this region and (b) exhibits considerable complexity as shown in

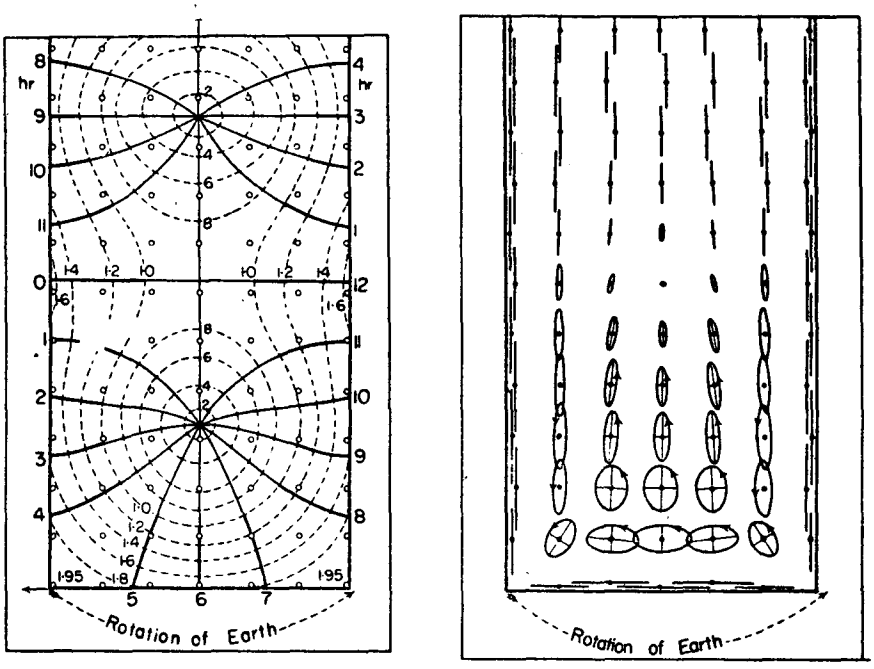

FIG. 9. Total reflection of a Kelvin wave at the closed lower end of a rectangular basin (Taylor, 1920). Cotidal (solid) and corange (dashed) lines are shown at the left and the corresponding current ellipses at the right (after Defant, 1961).

Fig. 2. Actual computations show there is considerable along and across-isobath curvature (not easily inferred from Fig. 2) in the tidal pressure-gradient field which is probably responsible for the large difference in tidal-current ellipse shapes found at stations NE2 and NE2W (see Fig. 3).

On a "typical" shelf region like that found off New Jersey the Clarke and Battisti (1981) and the Battisti and Clarke (1982) diagnostic models can be used to make good predictions of tidal elevation and currents at any shelf location with just a knowledge of the local coastal sea levels and across-shelf bathymetry. Unfortunately a principal assumption of those models is that the along-shelf (isobath) pressure gradient is uniform in the across-shelf direction. So although the tides in our study region are qualitatively similar to those in typical shelf regions (e.g., the New Jersey shelf) with some shoreward amplification commensurate with the local shelf width and clockwise rotary current ellipse, we would not expect quantitative agreement between observations and model predictions. Thus a more complete theoretical treatment of shelf tides incorporating across-shelf structure in the along-shelf pressure gradient is required—an exercise beyond the scope of this work.

b. Comparison of observations and numerical results

In this section we describe a comparison between the observations considered here and results from the fine grid ($\Delta x = \Delta y = 7.41$ km) depth-averaged numerical tidal model of the Gulf of Maine–Bay of Fundy system developed by Greenberg (1983). The appropriate M_2-constituent model results, which have been kindly provided by D. Greenberg, are compared in Table 1 with observed bottom pressures and depth-averaged currents from each Georges Bank and western Gulf station.

We find excellent agreement between the model and observed pressure phases at all Bank and Gulf stations. The Bank pressure amplitudes compare well with the exception of the station M3 model amplitudes which are about 10% less than observed. The model pressure amplitudes in the Gulf on the other hand are systematically greater (about 6%) than observed amplitudes, which have uncertainties of about ±1%. These Gulf pressure amplitude results are somewhat unexpected because the model has been tuned to reproduce both observed coastal tides around the Gulf and several sets of observed bottom pressures including these western Gulf observations and others from Georges Bank.

In general, the model current amplitudes are significantly less than their observed counterparts on the Bank and conversely significantly greater than their Gulf counterparts even after considering the approximate ±10% uncertainties in our computed depth-averaged current amplitudes (see Table C1, Appendix C). As we found with the pressures, the phase comparisons are relatively better when the phase uncertainties in the observed currents are considered (see Table A2, Appendix A). The details of the model–observation comparisons at the Bank station M4 and

the Gulf station CL support the general descriptions made above and are probably the most reliable because of the relatively better vertical-structure information on the currents there.

The major differences between observed and model depth-averaged currents are probably due to a combination of inaccuracies in 1) the estimates of observed depth-averaged currents, 2) the resolution of model local depths and 3) the specification of model friction. Admittedly the uncertainty estimates for our observed depth-averaged currents as discussed in Appendix C are crude but the consistency of the Bank across-isobath transport at both the 80 and 44 m isobaths (Table 4) suggests that estimated uncertainties of ±10% are reasonable. Therefore we must consider potential uncertainties in the model computations in order to account for the differences. In lieu of a detailed examination of the model depth and bottom friction specifications (which are not available to us) we note the regional difference in the current and pressure results and suggest that inaccuracies in the specification of bottom friction are probably responsible for a significant part of the comparison differences. More conclusive statements regarding these differences await more complete analysis than is possible here.

The model pressures and currents from locations corresponding to our Georges Bank stations M3, M4 and M9 have been used in a dynamical computation identical to that presented in Section C. The model and observed results presented in Table 3 compare very well with the exception of the across-isobath inertial term and the along-isobath residual term. The good overall comparison is due in part to the compensating effects of the opposed inertial and Coriolis terms, which depend on the generally lower model currents.

The transition that occurs in the local tidal dynamics along a transect from the southern flank of Georges Bank to the western Gulf of Maine has been explored by computing the numerical-model phase difference between maximum sea level and across-isobath current. The presentation of the model results in Fig. 10 shows how the progressive-wave dynamics on the southern flank of the Bank are strongly modified by both the topography and energy dissipation at successive stations across the Bank. The transition to the standing-wave phase relationship of the Gulf occurs rather abruptly over about 20 km just north of the Bank. Consistent with our other results the model and observed phase differences compare well, indicating the usefulness of the model in providing detailed horizontal pictures of the tidal characteristics even in complicated regions.

Of course all model and observed results discussed thus far have concerned vertically averaged tidal currents. In the next section we will briefly discuss an example of the typical vertical structure of tidal currents on Georges Bank in terms of the role of bottom friction.

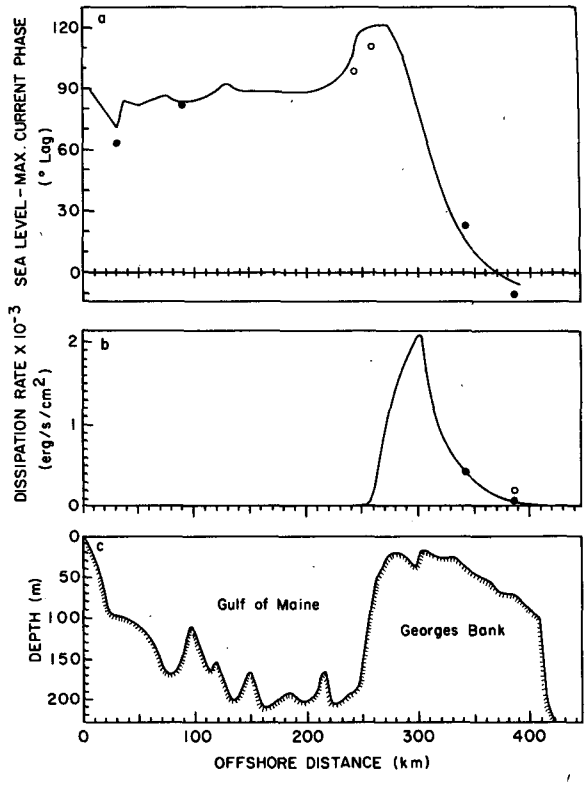

FIG. 10. The across-Bank and Gulf distribution of (a) the maximum M_2-tidal sea level/across-isobath current phase difference and (b) M_2-tidal energy dissipation rate computed by the Greenberg (1983) model. The bathymetry for the same transect is shown in (c). The Georges Bank stations M4, M3 and Gulf of Maine stations CL and MO phase difference results (solid circles) from this study are presented for comparison. An additional pair of data (open circles) were crudely estimated from the harmonic analyses of a single mid-depth tidal current and local sea level (Moody *et al.*, 1983) from each of two northern flank stations along the transect.

c. Three-dimensional considerations—Georges Bank

The clockwise-rotating M_2 tidal current ellipses found at the three levels at station M4 exhibit a significant shear which must be due in part to bottom friction. The time dependence of the shear is explored with a 12-lunar-hour sequence of across-isobath profiles which are compared in Fig. 11. These profiles have been constructed from station M4 tidal current analysis results plus an inferred current 1 m above the bottom (78 m depth) derived from Moody and Butman (1980) current observations near station M9. It can be seen there and perhaps even more clearly in the current hodograph sequence in Fig. 12 how the bottom current (and thus the bottom stress) leads the vertically averaged current for a particular profile. At $-\bar{U}_{max}$ the near-bottom current leads the 6 m current by about 30° and during the next quarter-tidal period (as $-\bar{U}$ decreases toward zero and $\bar{V}$ increases from near zero at $-\bar{U}_{max}$), the bottom current decreases in magnitude

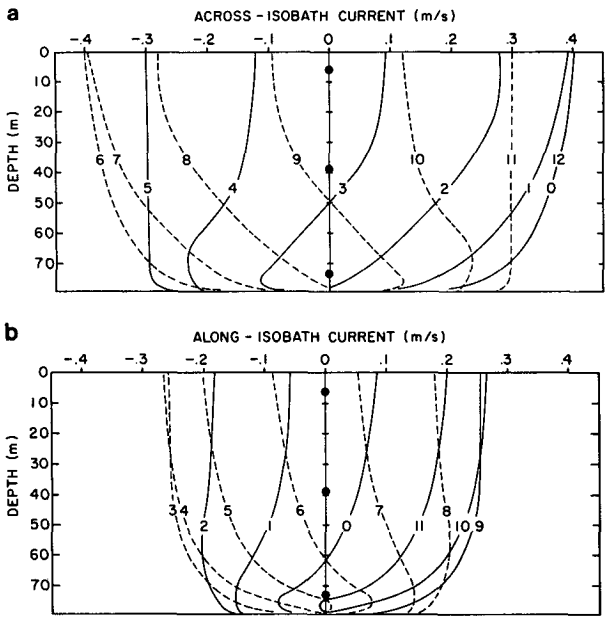

FIG. 11. A sequence of M_2 tidal current profiles from station M4 (79 m) on the southern flank of Georges Bank at lunar hourly (1.035 h) intervals. The predicted (a) across-isobath (330°T) and (b) along-isobath (240°T) currents at the observed depths (dots on zero axis) were used along with near-bottom current information from a nearby location reported by Moody and Butman (1980) to construct these profiles which are clearly influenced by the effects of bottom friction. The profiles for the first half (solid line) and the second half (dashed line) of the tidal cycle (referenced to maximum on-bank flow at 0 h) have been differentiated for readers convenience.

and sweeps through a clockwise change of nearly 120° so that at $+\bar{V}_{max}$ it leads the 6 m current by nearly 67°. During the next quarter-tidal period, the near-bottom current increases in magnitude as it sweeps more slowly through only ~60° to its direction at the time $+\bar{U}_{max}$. This description suggests an asymmetric (nonsinusoidal) temporal variability in the bottom current and a corresponding bottom stress which contrasts with the behavior of the other dynamical terms (see Fig. 4).

We can gain some insight into the dynamics of this sheared tidal flow by considering the work of Tee (1979) which describes a study of the vertical structure of shallow-water tidal currents. He partitions the analysis into a depth-averaged part, which contains pressure gradient effects and bottom friction, and a depth-dependent part, which contains the effects of internal friction. The two analyses are linked through the value of bottom stress which appears in each part. In comparing Tee's (1979) and our Georges Bank station M4 normalized velocity profiles, we find, as shown in Fig. 13, encouraging evidence that Tee's results will be generally applicable to the dynamical conditions at M4. This conclusion is reinforced by the favorable comparison between the station M4 results from 79-m depth and the 19-m-depth results of Bowden and Fairbairn (1952) which we present here in a composite of Tee results (Fig. 13).

Tee's (1979) model results depend on his use of different specifications for the vertical structure of eddy viscosity as summarized in panel (c) of Fig. 13. The maximum vertical eddy viscosity N_m characterizing each of these structures, can be computed for a particular tidal environment according to the relation $N_m \equiv (\sigma/2)(D/d_0)^2$, where the M_2 tidal frequency is $\sigma = 1.405 \times 10^{-4}$ s^{-1}, D is the water depth and d_0 a dimensionless friction scale. For each of the viscosity models Tee presents a relation between d_0 and a normalized friction coefficient, λ/σ, where $\lambda \equiv K\gamma U_m/D$ for which U_m is the depth-averaged current ellipse semimajor axis, $K = 0.95$ and $\gamma = 2.1 \times 10^{-3}$ (Bowden *et al.*, 1959). Tee finds that these relations, which appear in his Fig. 2, are relatively insensitive to depth, so that we are able first to find the d_0s for the conditions at stations M3, M4, M9 and the volume integrated results and then to compute the corresponding N_m values (see Table 5). For the sublayer and combined eddy-viscosity models the computed N_m values are within a factor of 2 for a range of depths between 19 and 79 m and provide additional evidence of the general usefulness of Tee's model in providing three-dimensional information on the basis of just depth-averaged currents.

In summary, we conclude from this brief analysis that 1) our observations are most consistent with Tee's (1979) sublayer ($\delta_z = 0.1$ m) and combined ($\delta_z = 0.07$ m, $R_1 = 0.5$ m) eddy-viscosity model results and 2) Tee's dynamical model can be used in conjunction

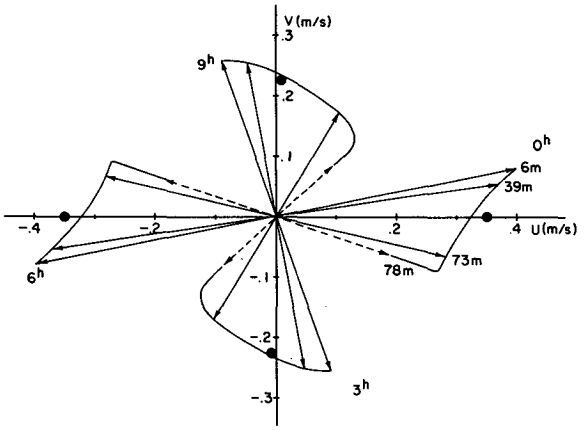

FIG. 12. A sequence of M_2 tidal current hodographs from station M4 (79 m) on the southern flank of Georges Bank at 3 lunar hourly (3.105 h) intervals. The predicted currents at 6, 39 and 73 m depth have been plotted on a rotated coordinate system with the across-isobath direction (X) and along-isobath direction (Y) of 330 and 240°T respectively. Also shown are near-bottom current vectors (dashed lines) which have been estimated from current information reported by Moody and Butman (1980). This presentation shows the relation between the instantaneous depth-averaged current (dots) and the vertical distribution of M_2 tidal current at quarterly intervals through the tidal cycle.

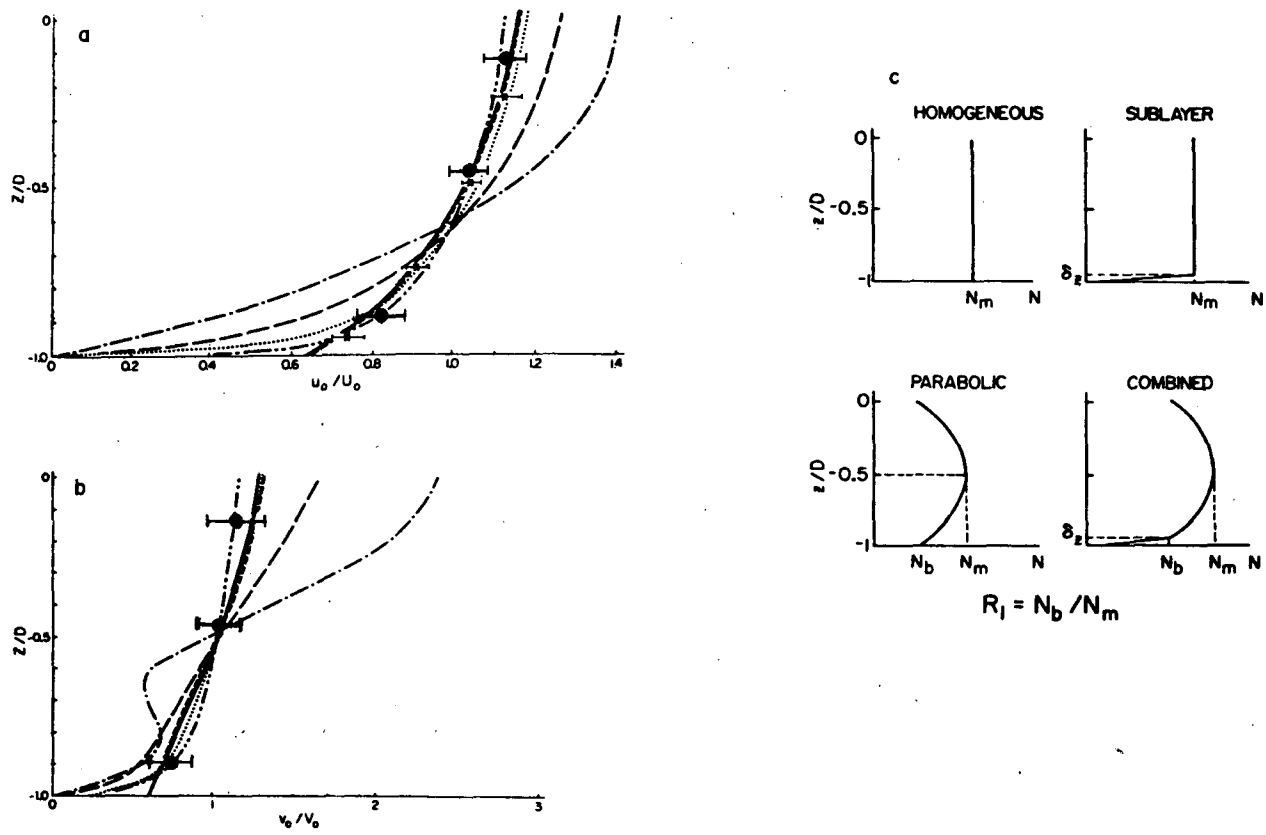

FIG. 13. A comparison of the predicted M_2 tidal current amplitudes from Georges Bank station M4 (dot-range bar) in 77 m of water with model current profiles computed by Tee (1979) for a variety of viscosity models. The vertical variation of tidal currents amplitudes (u_0, v_0) normalized by the depth averaged current amplitudes (U_0, V_0) are shown in panels (a) and (b) respectively for the viscosity models in panel (c): homogeneous; (dot-dash) parabolic, $R_1 = 0.1$; (dot) parabolic, $R_1 = 0.01$; (double dot-dash) parabolic, $R_1 = 0.001$; (dash) sublayer, $\delta_z = 0.1$ m; (solid) combined $\delta_z = 0.07$ m, $R_1 = 0.5$ m. Note how well the Georges Bank results (77 m depth) compare with the Bowden and Fairbairn (1952) results (19 m depth) (×-range bar). (A composite from Tee, 1979).

with observed or model depth-averaged currents to provide both vertical structure information and accurate estimates of local energy dissipation as desired.

d. Tidal energy dissipation rate—Georges Bank

One of the several ways of estimating tidal energy dissipation rate from flow conditions is to form the product of an estimated bottom stress $\tau_b{}^L$ using a "linear" drag law and the depth-averaged tidal velocity $\mathbf{U} = u\mathbf{i} + v\mathbf{j}$. According to Tee (1979) $\tau_b{}^L$ can be computed according to

$$\tau_b{}^L = \rho\lambda D\mathbf{U} = C_D\mathbf{U},$$

where the variable friction coefficient is $\lambda = k\gamma U_m/D$; k ranges from $\frac{8}{3\pi}$ to 1 as the ellipticity varies from 0 to 1 (circle), $\gamma = 2.1 \times 10^{-3}$, and U_m is the amplitude (semimajor ellipse axis) of the depth-averaged flow. Thus

$$C_D = \rho\lambda D = \rho K\gamma U_m,$$

with $K = 0.95$, $\gamma = 2.1 \times 10^{-3}$ and $\rho = 1.025$ gm cm^{-3}, becomes

$$C_D = 2.0 \times 10^{-3}U_m.$$

The corresponding dissipation rate Φ^L is then computed according to

$$\Phi^L = \tau_b{}^L \cdot \mathbf{U} = C_D(u^2 + v^2)$$

so that the time-averaged dissipation rate $\overline{\Phi^L}$ for sinusoidal velocity components is

$$\overline{\Phi^L} = \tfrac{1}{2}C_D(u_0{}^2 + v_0{}^2),$$

where u_0 and v_0 are the amplitudes of the across- and along-isobath components of the M_2 tidal current given in Table 1. The dissipation rates $\overline{\Phi^L}$ for Georges Bank stations M3 and M4 are compared with Greenberg's (1983) numerical-model dissipation rates $\overline{\Phi^G}$ at corresponding locations in Table 5 and in Fig. 10. The similarity in $\overline{\Phi^L}$ and $\overline{\Phi^G}$ just confirms that similar

TABLE 5. Tidal dynamics-model (Tee, 1979) maximum eddy viscosities N_m ($m^2\ s^{-1}$) for Georges Bank stations M3, M4, M9 and volume integrated currents (VOL) are compared with Tee's N_m values for Bowden and Fairbairn's (1952) observations at Station West. The Georges Bank values are based on the use of a dimensionless friction coefficient ($\lambda/\sigma = K\gamma U_m/\sigma D$) where $K = 0.95$ and $\gamma = 2.1 \times 10^{-3}$ (Bowden *et al.*, 1959) are friction coefficients, U_m is the depth-averaged current ellipse semimajor axis, D the water depth and $\sigma = 1.405 \times 10^{-4}$ s^{-1} is the semidiurnal frequency. The dimensionless frictional depth scale d_0 is found for each model from Tee's (1979) Fig. 2 on the basis of λ/σ. The model eddy viscosity is computed according to $N_m = (\sigma/2)(D/d_0)^2$.

Station	M3		M4		M9		VOL		West	
$D(m)$	44		79		81		62		19	
λ/σ	0.216		0.065		0.070		0.110		—	
Eddy viscosity model	d_0	$N_m \times 10^4$	d_0	$N_m \times 10^4$	d_0	$N_m \times 10^4$	d_0	$N_m \times 10^4$	d_0	$N_m \times 10^4$
Homogeneous	31	142	~7	85	~6	122	5	105	2.0	65
Parabolic $R_1 = 0.001$	1.2	944	2.1	944	2.0	1096	1.6	1021	0.8	367
Sublayer $\delta_Z = 0.1$ m	1.9	377	4.9	173	4.7	198	3.1	272	1.2	182
Combined $\delta_Z = 0.07$ $R_1 = 0.5$	1.8	420	4.3	225	4.1	261	2.8	333	1.1	218

methods have been used for the computation (we have already shown that both observed and model tidal currents compare well).

Ippen (1966) shows that a single component of the average dissipation rate $\overline{\Phi_x^I}$ for long waves can be computed according to

$$\overline{\Phi_x^I} = \frac{1}{T}\int_0^T \int_{-h} \rho N(z)\left(\frac{\partial u}{\partial z}\right)^2 dz dt,$$

where $N(z)$ is the eddy viscosity and T in this equation is the wave period. Here we estimate the average dissipation rate for station M4 using predicted M_2 currents and Tee's (1979) sublayer eddy-viscosity specification for $N(z)$ which is a constant value $N = N_m = 173$ $cm^2\ s^{-1}$ from Table 5. Applying Simpson's-rule, integration formulation to 48 ¼-lunar hourly samples of each predicted current component we estimate an across-isobath $\overline{\Phi_x^I} = 141.8$ ergs $cm^{-2}\ s^{-1}$ and an along-isobath $\overline{\Phi_y^I} = 57.1$ ergs $cm^{-2}\ s^{-1}$. Thus the total M_2-tidal-current dissipation rate $\overline{\Phi^I} = \overline{\Phi_x^I} + \overline{\Phi_y^I} = 198$ ergs $cm^{-2}\ s^{-1}$, which, as Table 6 shows, is about four times greater than estimated using a depth averaged current and a linear bottom stress.

Thus there is the suggestion that numerical estimates of tidal dissipation rates in some locations could be in error by significant amounts. Inasmuch as the near-resonant physics of the Gulf of Maine–Bay of Fundy tides is probably sensitive to the dissipation rates, the resolution of such differences could be an important step in the refinement of predictions of how the Gulf's tidal response will change with the installment of tidal power generation facilities.

TABLE 6. A comparison of average M_2 tidal energy dissipation rate (ergs $cm^{-2}\ s^{-1}$) estimates at stations M4 and M3. $\overline{\Phi^L}$ is computed using a linear bottom stress law (see text), $\overline{\Phi^G}$ is computed by Greenberg's (1983a) fine-grid numerical tidal model and $\overline{\Phi^I}$ has been estimated using Ippen's (1966) relation (see text).

Station	$\overline{\Phi^L}$	$\overline{\Phi^G}$	$\overline{\Phi^I}$
M4	55	50	198
M3	431	400	—

5. Concluding remarks

A rigorous method for estimating the volume-integrated tidal dynamics of a general continental shelf region from observations has been presented. Its application to three distinctly different regimes on the northeast American continental shelf shows that the M_2 semidiurnal tidal response 1) on Georges Bank is consistent with forced gyroscopic-progressive wave dynamics over a sloping bottom, 2) in the western Gulf of Maine is consistent with forced standing-Kelvin wave dynamics, and 3) on the New England Shelf, which lies in a tidal transition region between Georges Bank and the more typical New Jersey shelf, is not easily described because of the influence of complicated curvature in the along-shelf tidal pressure gradient.

A detailed comparison of these results with Greenberg's (1983) numerical model results for the Georges Bank–Gulf of Maine region resulted in good overall correspondence, but with some evidence that some refinement in the specification of model friction would improve the comparison.

A crude comparison of observed tidal-current profile results with Tee's (1979) model results provides evidence that such models may be a very useful complement to depth-averaged numerical results by providing information on the vertical structure of energy dissipation associated with shallow water (less than 100 m) tidal currents. Significant differences in results

TABLE A1. The principal tidal harmonic constituents for the bottom-pressure observations on Georges Bank, the Gulf of Maine and the New England shelf. The amplitudes H and Greenwich phases G are in millibars and degrees and station water depths are in meters. A discussion of the 95% confidence limits ascribed to the M_2 and K_1 constituents is given in Brown *et al.* (1982). A comparison of the standard deviations of the observed (OBS), residual (RES) and predicted M_2-series (M_2) (see text) appears in the right-hand columns.

	Station				Semidiurnal								Diurnal						Standard deviation		
	Position				M_2		S_2		N_2		M_2 95%		O_1		K_1		K_1 95%				
ID	Lat	Long	Depth	Days	H	G	H	G	H	G	H	G	H	G	H	G	H	G	OBS	M_2	RES
M3	41.33	67.25	44	122	39.6	22	9.8	15	10.0	354	±0.8	±0.9	6.6	179	6.6	178	±0.7	±5.0	32.2	28.0	4.5
M4	40.92	66.97	79	266	38.5	1	8.4	26	10.1	349	±0.8	±0.9	5.8	185	7.5	168	±0.6	±4.3	31.8	27.2	3.6
M9	40.89	67.39	81	316	38.9	6	7.9	32	10.7	346	±0.9	±1.1	5.6	188	7.2	170	±0.9	±4.7	31.6	27.5	4.2
CP	43.22	70.28	98	73	127.8	103	20.4	134	30.0	71	±1.2	±0.5	10.7	185	13.0	204	±0.9	±3.8	94.8	89.5	11.5
MO	43.67	69.38	98	56	131.3	99	21.2	128	30.5	67	±1.2	±0.5	10.4	181	13.7	198	±0.9	±3.5	98.5	92.6	10.7
CL	43.18	69.08	190	57	120.7	98	19.6	126	28.3	66	±1.2	±0.5	10.2	186	12.6	198	±1.0	±4.1	90.9	85.2	10.4
A4	40.57	72.30	50	61	48.3	346	11.5	12	12.1	329	±1.0	±1.1	5.1	178	8.4	168	±0.8	±5.2	43.6	34.2	19.8
A5	40.19	72.00	67	183	47.0	349	10.5	15	11.3	331	±0.6	±0.5	6.0	185	8.3	175	±0.3	±2.0	37.8	33.2	8.9
P	40.72	71.32	60	36	43.5	348	9.5	10	10.4	331	±0.8	±0.9	5.2	188	7.5	166	±0.5	±3.8	33.8	30.8	5.5
K	39.93	71.05	509	48	42.5	347	9.2	15	10.0	327	±0.5	±0.6	7.2	181	9.1	177	±0.4	±2.3	32.6	30.1	2.2

of alternate ways of computing tidal energy dissipation suggests that this whole area of inquiry needs more attention.

Acknowledgments. The basis of the Georges Bank work presented here were some of the observations obtained by EG&G Environmental Consultants, Inc. (Waltham, Mass.) under contract to the Bureau of Land Management, while the data in the Gulf of Maine and New England Shelf were obtained by R. C. Beardsley and J. Vermersch (WHOI) and provided to the author. Additional bottom pressure records from south of Long Island were provided by H. Mofjeld (NOAA, PMEL). Special assistance was provided by J. D. Irish (UNH), who under subcontract to EG&G reduced and achieved the pressure and the current data, helped in the development of the tidal harmonic analyses and provided helpful comment on the manuscript. Helpful comments regarding earlier versions of this manuscript were provided by B. Butman, R. C. Beardsley, B. Magnell, A. J. Clarke and an anonymous reviewer. This work was supported in part by a subcontract to EG&G and by the National Science Foundation through Grant OCE 8014940.

APPENDIX A

Tidal Harmonic Constants

Harmonic constants have been computed for the pressures and currents used in this study using a method adapted from the National Ocean Survey (NOS) method described by Dennis and Long (1971). In Table A1 the pressure amplitudes and Greenwich phases of the three main semidiurnal constituents M_2 (principal lunar), S_2 (principal solar) and N_2 (larger lunar elliptic) and the two main diurnal constituents O_1 (principal lunar) and K_1 (luni-solar) are listed along with the estimated 95% confidence limits for the M_2 and K_1 constituents. In addition the standard deviations for the full series, full series minus a predicted series (residual series) and a predicted M_2 series are compared. In Table A2 the across- and along-isobath current component amplitudes and Greenwich phases and corresponding supporting information are listed, where significant, for the same five harmonic constituents.

APPENDIX B

Vertical Integral Estimates

A summary of methods used to estimate the vertical integrals of across-isobath $\bar{u}$ and along-isobath $\bar{v}$ current at each station from the component currents at the depths indicated by the subscripts in Table B1. At stations M3, M9 and CP the single current has been adjusted in amplitude (and phase for M9) by the factors in parentheses (see text) to produce the vertically integrated current estimate in units of $m^2\ s^{-1}$.

TABLE A2. The principal tidal harmonic constituents for the current observations on Georges Bank, the Gulf of Maine and the New England shelf. The local across-isobath (X) and the along-isobath (Y) directions (DIR) relative to true north for each region are: 330°, 240° for Georges Bank; 324°, 234° for the Gulf of Maine and 340°, 250° for the New England shelf, respectively. Station and instrument water depths (DEP) are given in meters. The amplitudes H and Greenwich phases G are in cm s^{-1} and deg. A discussion of the 95% confidence limits ascribed to the M_2 and K_1 constituents is given by Brown *et al.* (1982). A comparison of the standard deviations of the observed (OBS), residual (RES) and predicted M_2-series (M_2) appears in the right-hand columns. The diurnal tidal currents for the western Gulf of Maine were too small to be resolved.

Station data					Instrument data		Semidiurnal								Diurnal						Standard deviation		
	Position						M_2		S_2		N_2		M_2 95%		O_1		K_1		K_1 95%				
ID	Lat	Long	Days	DEP	DEP	DIR	H	G	H	G	H	G	H	G	H	G	H	G	H	G	OBS	M_2	RES
M3	41.33	67.25	58	44	36	X	58.8	2	9.1	40	14.0	338	±1.0	±0.9	2.2	26	4.2	41	±0.2	±3.0	45.7	41.5	3.3
						Y	41.9	272	5.5	303	10.0	239	±0.9	±1.1	2.4	287	6.3	299	±0.4	±3.1	32.9	29.6	3.4
M4	40.92	66.97	58	79	6	X	39.4	25	3.5	50	8.7	351	±2.2	±2.9	1.0	321	3.2	38	±1.1	±18.9	32.1	27.9	10.9
						Y	26.0	298	3.5	300	5.5	251	±2.0	±4.1	1.9	306	4.6	314	±1.1	±12.6	22.6	18.3	10.4
					39	X	35.9	18	6.1	55	9.1	4	±1.5	±2.1	1.8	57	3.7	46	±1.8	±27.5	30.2	25.5	10.8
						Y	24.7	292	4.4	321	6.3	260	±1.7	±3.6	2.8	329	3.9	327	±1.2	±18.3	22.5	17.5	11.2
					73	X	28.7	351	1.9	37	6.4	327	±2.2	±4.1	1.7	77	2.7	97	±0.9	±18.3	23.6	20.3	8.3
						Y	18.2	259	0.8	294	4.6	221	±1.6	±4.8	1.2	310	2.9	352	±0.8	±16.0	16.3	12.9	8.0
M9	40.89	67.39	58	81	75	X	32.7	352	5.2	56	5.6	318	±1.4	±2.2	0.7	62	1.9	99	±0.6	±18.3	26.0	23.3	6.9
						Y	18.6	251	2.6	318	3.2	214	±1.1	±3.1	0.9	282	2.7	357	±0.6	±13.2	15.4	12.8	6.7
CP	43.22	70.28	73	98	33	X	5.2	352	0.5	10	1.1	324	±0.4	±3.7	—	—	—	—	—	—	6.7	3.7	5.5
						Y	3.5	117	0.6	115	1.0	73	±0.5	±7.5							8.0	2.5	7.6
MO	43.67	69.38	56	98	33	X	5.7	21	0.9	61	1.1	343	±0.3	±3.0	—	—	—	—	—	—	6.4	4.0	4.9
						Y	6.4	148	0.8	164	1.4	106	±0.4	±3.1							8.2	4.5	6.6
					68	X	2.6	70	0.2	78	1.0	235	±0.8	±17.2	—	—	—	—	—	—	4.6	1.8	4.2
						Y	4.6	184	0.4	215	0.9	134	±1.3	±11.5							5.9	3.3	4.7
CL	43.18	69.08	57	190	33	X	13.4	26	1.7	52	2.5	3	±0.7	±2.6	—	—	—	—	—	—	13.9	9.5	9.7
						Y	5.1	127	1.5	158	2.1	58	±0.7	±7.5							12.8	3.6	12.1
					68	X	8.4	33	1.5	30	1.9	12	±0.7	±4.4	—	—	—	—	—	—	8.5	5.9	5.8
						Y	3.4	122	6.6	120	0.9	57	±0.5	±7.6							6.4	2.4	5.8
					48	X	9.5	5	1.9	47	1.8	336	±0.5	±2.6	—	—	—	—	—	—	8.8	6.7	5.2
						Y	4.2	109	0.5	104	0.8	69	±0.4	±4.5							5.8	3.0	4.8
NE2	40.36	71.20	89	83	38	X	6.2	304	1.7	315	1.6	287	±0.5	±3.9	1.8	46	2.9	106	±0.5	±8.2	8.7	4.4	6.7
						Y	5.9	219	1.3	238	1.4	181	±0.4	±3.2	3.2	336	3.7	22	±0.6	±8.3	10.8	4.2	9.3
NE2W	39.98	71.96	89	83	38	X	8.0	273	2.0	296	2.0	265	±0.6	±3.8	2.5	117	2.2	160	±0.7	±17.8	8.9	5.7	6.0
						Y	6.2	209	1.6	224	1.7	197	±0.5	±4.1	3.5	16	3.2	71	±0.9	±16.0	11.2	4.4	9.7

TABLE B1.

Site	Station	Vertical integral estimate
Georges Bank	M3	$\bar{u} = (1.10)44u_{36}$ $\bar{v} = (1.20)44v_{36}$
	M4	$\bar{u} = 22.0u_6 + 33.5u_{39} + 23.0\ u_{73}$ $\bar{v} = 22.0v_6 + 33.5v_{39} + 23.0v_{73}$
	M9	$\bar{u} = (1.15)81u_{75}$ (lagged by 1 h) $\bar{v} = (1.24)81v_{75}$ (lagged by 1 h)
Gulf of Maine	CP	$\bar{u} = (0.67)98u_{33}$ (lagged by 0.5 h) $\bar{v} = (0.80)98v_{33}$ (lagged by 0.5 h)
	MO	$\bar{u} = 50u_{33} + 48u_{68}$ $\bar{v} = 51v_{33} + 48v_{68}$
	CL	$\bar{u} = 50u_{33} + 43u_{68} + 97u_{118}$ $\bar{v} = 50v_{33} + 43v_{68} + 97v_{118}$
New England shelf	NE2	$\bar{u} = 83u_{38}$ $\bar{v} = 83v_{38}$
	NE2W	$\bar{u} = 83u_{38}$ $\bar{v} = 83v_{38}$

APPENDIX C

Uncertainty Estimates of Stress Balance Terms

The following is a discussion of how the uncertainty limits for each of the terms in the stress-balance have been estimated. In each case an attempt has been made to account separately for the uncertainty associated with 1) making observations in the ocean and computing predictions based on those observations and 2) making estimates of integral and differential terms in Eqs. (10) and (11) of the main text. In particular, we outline below the methods used to estimate uncertainty limits associated with the computation of the volume-integrated velocity, [V], and the other momentum terms for the M_2-series input. A major assumption in these discussions is that errors associated with the uncertainties are uncorrelated with the signal and with each other unless otherwise stated.

1. Vertically integrated velocity

Here a single *component* of the vertical integral of velocity $\bar{V}$ is described in terms of its true value $\bar{V}_T$ and an uncertainty ϵ_s according to

$$\bar{V} = \bar{V}_T \pm \epsilon_s, \tag{C1}$$

where

$$\epsilon_s^2 = \epsilon_{VI}^2 + \epsilon_R^2 \tag{C2}$$

and it is assumed that the measurement uncertainties ϵ_R and the integration-estimate uncertainties ϵ_{VI} are due to independent random errors. In this computation we use Simpson's rule to estimate vertical integrals from the measured currents according to

$$\bar{V} = \sum_i a_i V_{mi}, \tag{C3}$$

where a_i are the weights associated with the ith level current V_{mi} as presented in Appendix B. Each current is described by the sum of its true value and a random computational uncertainty ϵ_{mi} given in Table A2 of Appendix A so that ϵ_R can be estimated according to

$$\epsilon_R^2 = \sum_i (a_i\epsilon_{mi})^2. \tag{C4}$$

By comparing estimates using Simpson's rule with those made using logarithmic and piece-wise linear fits, we find that the typical normalized uncertainty in our integration process $\hat{\epsilon}_{VI}$ for M_2 currents is about ±4% for Georges Bank. So for ϵ_R^2 computed according to (C4) we find the normalized overall uncertainty of the vertically integrated currents $\hat{\epsilon}_s$ as listed in Table C1 for each station.

2. Horizontally integrated current

As with vertical integrals, horizontally integrated components are described by

TABLE C1. Normalized uncertainties ($\hat{\epsilon}_R$ and $\hat{\epsilon}_s$) for vertically integrated currents computed for the M_2-series according to equations (C4) and (C2).

Station		$\pm\hat{\epsilon}_R$	$\pm\hat{\epsilon}_s$	σ_V	$\pm\epsilon_{sj}$
M3	X	0.016	0.044	20.8	0.92
	Y	0.021	0.047	16.0	0.75
M4	X	0.032	0.051	18.9	0.96
	Y	0.045	0.060	12.4	0.74
M9	X	0.041	0.057	22.2	1.27
	Y	0.059	0.071	13.1	0.93
CP	X	0.075	0.085	2.5	0.21
	Y	0.140	0.146	1.9	0.28
MO	X	0.120	0.126	2.7	0.34
	Y	0.131	0.137	3.6	0.49
CL	X	0.035	0.053	13.9	0.74
	Y	0.071	0.081	5.6	0.45
NE2	X	0.078	0.088	3.8	0.33
	Y	0.066	0.078	3.5	0.39
NE2W	X	0.083	0.092	4.3	0.27
	Y	0.078	0.088	3.7	0.33

$$[V] = [V]_T \pm \epsilon_{ss}, \quad \text{(C5)}$$

where the squared uncertainty in $[V]$ is given by

$$\epsilon_{ss}^2 = \epsilon_{HI}^2 + \epsilon_{RR}^2. \quad \text{(C6)}$$

Here ϵ_{HI}^2 is the squared integration error and ϵ_{RR}^2 contains the propagated form of the ϵ_s uncertainties. The ϵ_{RR}^2 is computed according to

$$\epsilon_{RR}^2 = \sum_j (b_j \epsilon_{sj})^2, \quad \text{(C7)}$$

where b_j are the weights presented in Table 2 for computing the $[V]$s, from $\bar{V}$s at the jth station and the ϵ_{sj}s are the corresponding uncertainties (see Table C1 for their values). The normalized form of ϵ_{RR} for the Bank computation is

$$\hat{\epsilon}_{RR} = \frac{\epsilon_{RR}}{\sigma_{[V]}} = [(0.25\epsilon_{s\mathrm{M4}})^2 + (0.25\epsilon_{s\mathrm{M9}})^2 + (0.5\epsilon_{s\mathrm{M3}})^2]^{1/2} \frac{\Delta x \Delta y}{\sigma_{[V]}}, \quad \text{(C8)}$$

where $\sigma_{[V]}$ is the standard deviation of the volume integrated velocity. For the Bank computation ϵ_{HI} is estimated from the difference between the integrated form of a Taylor expansion of the vertical integral of velocity about station M4 ($\bar{V}_{\mathrm{TAYLOR}}$) and the actual computation ($\bar{V}_{\mathrm{COMPUTED}}$) according to

$$\epsilon_{HI} = 0.5(\bar{V}_{\mathrm{TAYLOR}} - \bar{V}_{\mathrm{COMPUTED}}),$$

where

$$\left.\begin{aligned} \bar{V}_{\mathrm{TAYLOR}} &= \bar{V}_{\mathrm{M4}} \Delta x \Delta y 0.5 \left.\frac{\partial \bar{V}}{\partial x}\right|_y \Delta x^2 \Delta y \\ &\quad + 0.5 \left.\frac{\partial \bar{V}}{\partial y}\right|_x \Delta x \Delta y^2 + \cdots \\ \bar{V}_{\mathrm{COMPUTED}} &= [0.25(\bar{V}_{\mathrm{M4}} + \bar{V}_{\mathrm{M9}}) \\ &\quad + 0.5\bar{V}_{\mathrm{M3}}]\Delta x \Delta y \end{aligned}\right\}.$$

The normalized error form of (C8) is

$$\hat{\epsilon}_{HI} = \frac{\epsilon_{HI}}{\sigma_{[V]}} = [0.5(0.75\bar{V}_{\mathrm{M4}} - 0.5\bar{V}_{\mathrm{M3}} - 0.25\bar{V}_{\mathrm{M4}}) + 0.5\delta_x\bar{V} + 0.5\delta_y\bar{V}] \frac{\Delta x \Delta y}{\sigma_{[V]}}, \quad \text{(C9)}$$

TABLE C2. The M_2-series normalized uncertainty estimates for the volume integral of currents.

		$\pm\hat{\epsilon}_{RR}$	$\pm\hat{\epsilon}_{HI}$	$\pm\hat{\epsilon}_{ss}$
Georges Bank	X	0.030	0.085	0.090
	Y	0.034	0.072	0.080
Gulf of Maine	X	0.046	~0.100	0.110
	Y	0.069	~0.080	0.106
New England shelf	X	0.055	0.120	0.132
	Y	0.070	~0.100	0.122

where gradients are approximated by finite differences $\delta_x\bar{V}/\Delta x$ and $\delta_y\bar{V}/\Delta y$ respectively.

The normalized errors associated with the M_2-series volume integrated velocity [V] are computed using (C6), (C8) and (C9) and are presented in Table C2.

3. Inertial term

Here a component of the inertial term is described in terms of its true value and two uncertainty terms according to

$$\frac{\delta[V]}{\delta t} = \frac{\partial[V]^T}{\partial t} \pm \epsilon_I + \epsilon_{DI}, \quad \text{(C10)}$$

where ϵ_I equals ϵ_{ss}, which is the random uncertainty of $[V]$, and ϵ_{DI} is the systematic underestimate of an oscillatory term due to the use of finite first-differencing techniques. This error can be corrected for as discussed below.

The systematic underestimate of the inertial term can be explored in general by writing the normalized form of ϵ_{DI} (i.e., $\hat{\epsilon}_{DI}$) in terms of the true differential V_t and the finite difference form $\Delta_t V$ according to

$$\hat{\epsilon}_{DI} = 1 - \Delta_t V / V_t. \quad \text{(C11)}$$

For a monochromatic input (i.e., $V = V_0 \sin\omega t$)

$$\Delta_t V = \frac{V(t + \Delta t) - V(t - \Delta t)}{2\Delta t},$$

which means that (A11) can be written

$$\hat{\epsilon}_{DI} = 1 - \frac{\sin\omega\Delta t}{\omega\Delta t}. \quad \text{(C12)}$$

This form shows that we always underestimate the amplitude of the inertial term by an amount $\hat{\epsilon}_{DI} \cdot \omega V_0$. For the M_2 frequency $\hat{\epsilon}_{DI}$ is 0.042 and we have amplified the computed inertial terms accordingly.

4. Nonlinear term

A typical nonlinear term for Georges Bank is proportional to the finite difference

$$\delta_y\overline{VV} = (\bar{V}_{\mathrm{M9}}\bar{V}_{\mathrm{M9}}) - (\bar{V}_{\mathrm{M4}}\bar{V}_{\mathrm{M4}}).$$

Hence the normalized uncertainty of a nonlinear term $\hat{\epsilon}_{NL}$ can be approximated as

$$\hat{\epsilon}_{NL} \sim [2(\epsilon_{\mathrm{SM9}}^2 + \epsilon_{\mathrm{SM4}}^2)]^{1/2}/\sigma_{\delta\overline{VV}},$$

where $\sigma_{\delta\overline{VV}}$ is the standard deviation of the Y-finite difference of $\overline{VV}$. This term is typically O(1) and thus the nonlinear terms, which are small anyway, have large uncertainties.

TABLE C3. The M_2-series normalized uncertainties associated with the different terms in the stress balance [see Eqs. (10) and (11) in text].

	Georges Bank		Gulf of Maine		New England shelf	
Term	X	Y	X	Y	X	Y
Inertial $\hat{\epsilon}_I = \hat{\epsilon}_{ss}$	±0.090	±0.080	±0.110	±0.106	±0.132	±0.122
Nonlinear $\hat{\epsilon}_{NL}$	±1.000	±1.000	±1.000	±1.000	—	—
Coriolis $\hat{\epsilon}_C = \hat{\epsilon}_{ss}$	±0.090	±0.080	±0.110	±0.106	±0.132	±0.122
Pressure gradient $\hat{\epsilon}_{PG}$	±0.093	±0.380	±0.154	±0.253	±0.827	±0.241
Residual $\hat{\epsilon}_{RS}$	±0.919	±0.660	±0.772	±0.350	±0.596	±1.049
Velocity $\hat{\epsilon}_V$	±0.090	±0.080	±0.110	±0.106	±0.132	±0.122

5. Coriolis term

Since the Coriolis terms are proportional to the volume integral of velocity $[V]$, we assume that the associated uncertainty of the Coriolis term will be proportional to the $[V]$ uncertainty such that

$$\hat{\epsilon}_C = \hat{\epsilon}_{ss}.$$

6. Pressure gradient term

Consistent with observations, we have assumed that the horizontal scales of the pressure field are so large that 1) a finite-difference and true differential forms of the pressure gradient are the same and 2) the variability of the pressure gradient components within the control volume leads to uncertainties that are small compared to those that arise when forming small first differences from large numbers.

This can be seen by considering the uncertainty associated with taking first differences between pressures, which are described in terms of the sum of a true value and random uncertainty term by

$$P_j = P_j^T \pm \epsilon_{pj},$$

where ϵ_{pj}s are the uncertainties of each pressure as given in Table A1. Pressure differences PD computed according to

$$PD = \sum_j C_j P_j,$$

where C_j are the weights, which can be determined from Table 1 and are used in finding the normalized uncertainty for the pressure difference $\hat{\epsilon}_{PD}$ according to

$$\hat{\epsilon}_{PD} = [\sum_j (C_j \epsilon_{pj})^2]^{1/2}/PD|_{\max}$$

where $PD|_{\max}$ is the amplitude of the pressure difference sinusoid. We assume that the normalized uncertainty of the pressure gradient term $\hat{\epsilon}_{PG}$ equals $\hat{\epsilon}_{PD}$.

The uncertainties ϵ_{pj} include instrumental noise which Brown *et al.* (1982) estimate to be ±0.0003 db from studies of Paroscientific pressure gauges. This is about 4% of the typical uncertainty and is an indication of the "contamination" of the astronomical tidal response due to other natural oceanic hydrodynamic processes.

7. Residual term

Finally we define the normalized error of the residual term $\hat{\epsilon}_{RS}$ according to

$$\hat{\epsilon}_{RS} = [(\sigma_I \hat{\epsilon}_I)^2 + 2(\sigma_{NL}\hat{\epsilon}_{NL})^2(\sigma_C \hat{\epsilon}_C)^2 + (\sigma_{PG}\hat{\epsilon}_{PG})^2]^{1/2}/\sigma_{RS}.$$

The values of the normalized uncertainties for each term at each site are presented in Table C3.

REFERENCES

Battisti, D. S., and A. J. Clarke, 1982: A simple method for estimating barotropic tidal currents on continental margins with specific application to the M_2 tide off the Atlantic and Pacific coasts of the United States. *J. Phys. Oceanogr.*, **12**, 8–16.

Beaumont, C., and R. Boutilier, 1978: Tidal loading of Nova Scotia: Results from and improved ocean tide model. *Can. J. Earth Sci.*, **15**, 981–993.

Bowden, K., and L. Fairbairn, 1952: A determination of the frictional forces in a tidal current. *Proc. Roy. Soc. London*, **A214**, 371–392.

——, —— and P. Hughes, 1959: The distribution of shearing stresses in tidal current. *Geophys. J. Roy. Astron. Soc.*, **2**, 288–305.

Brown, W. S., and R. C. Beardsley, 1978: Winter circulation in the western Gulf of Maine. Part I: Cooling and water mass formation. *J. Phys. Oceanogr.*, **8**, 265–277.

——, N. R. Pettigrew and J. D. Irish, 1982: Interpretation of the Physical Oceanography of Georges Bank. Final Report, Vol. 2, Appendix B; Tech. Rep. No. EG&G 82-B4569, 122 pp.

Clarke, A. J., and D. S. Battisti, 1981: The effect of continental shelves on tides. *Deep-Sea Res.*, **28**, 665–682.

Defant, A., 1961: *Physical Oceanography, Vol. 2.* Pergamon Press, 560 pp.

Dennis, R., and E. Long, 1971: A users guide to a computer program for harmonic analysis of data at tidal frequencies. NOAA Tech. Rpt. NOS41, 31 pp.

EG&G, 1979a: Data report, Eulerian studies, January 1978–February 1979, Appendix B, Tenth Quart. Prog. Rep. New England Outer Continental Shelf Physical Oceanography Program. EG&G, Environmental Consultants, Waltham, MA. 79 pp.

——, 1979b: Data report, Eulerian studies, April 1978–May 1979, Appendix B, Eleventh Quart. Prog. Rep. New England Outer Continental Shelf Physical Oceanography Program. 111 pp.

——, 1979c: Data report, Eulerian studies, March 1979–August 1979, Appendix B of the Twelfth Quart. Prog. Rep. New England Outer Continental Shelf Physical Oceanography Program. 108 pp.

——, 1980: Data report, Eulerian studies, November 1979–January 1980, Appendix B, Thirteenth Quart. Prog. Rep. New England

Outer Continental Shelf Physical Oceanography Program. 77 pp.

Garrett, C., 1972: Tidal resonance in the Bay of Fundy and Gulf of Maine. *Nature,* **238,** 441–443.

Greenberg, D. A., 1979: A numerical model investigation of tidal phenomena in the Bay of Fundy and the Gulf of Maine. *Mar. Geodesy,* **2,** 161–187.

——, 1983: Modeling the mean barotropic circulation in the Bay of Fundy and the Gulf of Maine. *J. Phys. Oceanogr.,* **13,** 886–904.

Ippen, A. T., 1966. *Estuary and Coastline Hydrodynamics.* McGraw-Hill, 744 pp.

Limburner, R., J. Vermersch and R. C. Beardsley, 1978: Hydrographic station data obtained in the vicinity of Georges Bank, May and August 1976, Tech. Rep. WHOI-78-83, WHOI, 116 pp.

Loder, J. W., 1980: Topographic rectification of tidal currents on the sides of Georges Bank. *J. Phys. Oceanogr.,* **10,** 1399–1416.

May, P. M., 1979: Analysis and interpretation of tidal currents in the coastal boundary layer. Doctoral dissertation WHOI/MIT Joint Program in Oceanography and Ocean Engineering, WHOI, 190 pp.

Moody, J. A., and B. Butnam, 1980: Moored current and bottom pressure observations of the semidiurnal tide on Georges Bank and in the Mid-Atlantic Bight, Open-File Rep. 80-1137, U.S. Department of Interior, U.S. Geol. Survey, 22 pp.

——, ——, R. C. Beardsley, W. S. Brown, P. Daifuku, D. A. Mayer, H. O. Mofjeld, B. Petrie, S. Ramp, P. Smith and W. R. Wright, 1983: Atlas of Tidal Elevation and Current Observations on the Northeast American Continental Shelf and Slope. U.S. Geological Survey Bulletin (U.S. Government Printing Office, Washington, DC) (in press).

Mysak, L. A., and C. L. Tang, 1974: Kelvin wave propagation along an irregular coastline. *J. Fluid. Mech.,* **64,** 241–261.

Ou, R., J. Vermersch, W. S. Brown and R. C. Beardsley, 1980: New England shelf/slope experiment (February to August, 1976) data report: The moored array. Tech. Rep. WHOI-80-3, WHOI, 59 pp.

Taylor, G. I., 1920: Tidal oscillations in gulfs and rectangular basins. *Proc. London Math. Soc.* (2), **20,** (Nos 2 and 3), 148–181.

Tee, K-T., 1979: The structure of three-dimensional tide-generating currents. Part I: Oscillating currents. *J. Phys. Oceanogr.,* **9,** 930–944.

Vermersch, J., R. C. Beardsley and W. S. Brown, 1979: Winter circulation in the western Gulf of Maine. Part 2: Current and pressure observations. *J. Phys. Oceanogr.,* **9,** 768–784.